The Characterization of Graphene Paper for Flexible Electronics Application

by

Kamyar Karimi

A thesis
presented to the University of Waterloo
in fulfillment of the
thesis requirement for the degree of
Master of Applied Science
in
Mechanical Engineering

Waterloo, Ontario, Canada, 2016

AUTHOR'S DECLARATION

I hereby declare that I am the sole author of this thesis. This is a true copy of the thesis, including any required final revisions, as accepted by my examiners. I understand that my thesis may be made electronically available to the public.

Abstract

Graphene has been gaining attention mainly because of its exceptional electrical and mechanical properties. Mono layer graphene with its planar hexagonal lattice structure is transparent and flexible. Together with its high electrical conductivity, this form of graphene can be an excellent material for flexible electronics. However, structural defects and lattice disorders have been the primary reasons for its inability to fulfill its full potential. As a result, other graphene based structures have been developed faster - one of the most important of which is graphene paper. Graphene paper is a hierarchical structure the building block of which is graphene nano platelets.

The objectives of the study were to synthesize high-quality graphene powder, and to prepare stable ink to fabricate graphene paper samples for electrical and mechanical characterization. Two types of tests were conducted to determine: (i) electrical resistance; and (ii) mechanical properties, specifically fatigue bending and adhesion. Experimental data were analyzed using standard statistical modeling techniques.

In this work, high quality graphene powder was first produced using liquid phase exfoliation. Then, stable graphene ink was developed to produce large scale graphene paper depositions on polyimide Kapton substrates. A large set of graphene paper samples was prepared with different ink concentration and annealed at a temperature range between 280 ^{o}C and 320 ^{o}C for periods for up to 24 hours.

The sheet resistance of the prepared graphene paper were measured using a custom built electrical fixture. The electrical measurement experiments indicated that the electrical resistance of graphene paper samples is mainly a function of annealing temperature, annealing time and concentration of the as-prepared ink.

A set of fatigue bending and adhesion tests was conducted to ensure that the material is mechanically durable such that the electrical resistance does not change after repeated bending loads. It was found that the material structure gets mechanically weaker as the annealing time increases. Prolonged annealing for periods longer than 8 hours at 300 ^{o}C degrades the mechanical properties of this specific graphene paper.

Finally, capacitance properties of the produced graphene paper were investigated. To simulate double layer capacitance behaviour, electrodes were fabricated with graphene paper coating and used

for cyclic voltammetry setup. It was found that the material does not exhibit ideal double layer behaviour due to its low porosity.

Keywords: graphene, graphene paper, electronic properties, mechanical properties, supercapacitor, statistical modeling.

Acknowledgements

First and foremost, I would like to thank my God without whom I was not here. I have been deeply feeling your presence and guidance since my childhood all the way through all the stages of my educational career. Thanks for being such a wonderful caring person, and I am completely sure you will share my confidence to be a successful person for the rest of my life.

I would like to express my sincere gratitude to my supervisor, Dr. Pearl Sullivan, who has patiently guided and encouraged me through my degree at the University of Waterloo. In spite of her hectic schedule as the dean of the engineering, she was the person who provided me with her ultimate support, and I will be grateful to her assistance for ever.

I would like to thank my co-supervisor, Dr. Ehsan Toyserkani for his technical assistance and providing the framework for this project.

I would like to thank Dr. Elahe Jabari for her trainings on material synthesis and her valuable recommendations which I used as a benchmark to build upon my experiments. Elahe: your time, attention and effort are greatly appreciated.

I would like to thank my colleague and my best friend, Siamak Ghorbani. As well as being a true supportive friend in these two years, without whom the material and electrochemical characterizations of this work would not be possible.

I would like to thank my colleges in Advanced Composite and Adhesive group, Dr. Allan Rogalsky and Geoff Rivers for their recommendations and trainings through this project.

I would like to thank Dr. Ehsan Marzbanrad for his time and valuable recommendations for my thesis.

I would like to thank Dr. Zhongwei Chen, Dr. Siva Sivoththaman for their permission to use their lab equipment which was invaluable to complete this study. This work would not be possible without the help of Mark Griffett, Sahar Hemmati, Gregory Lui and Bahareh Sadeghimakki.

Finally, my heartfelt gratitude goes to my beloved mom and dad. Taking all the challenges and responsibilities of a graduate student is one thing, having your family members far away in another country is totally another thing. Mom and Dad: you have been always holding the first place and will

be in the first place in my heart. I would not be here, and this work would not be possible without your continuous supports and encouragements throughout my whole life and more specifically in these two years from long distance. I wish you were here. Thank you for everything.

Dedication

I dedicate this work to my mom, Zahra, and dad, Davood, who mean everything to me.

Table of Contents

List of Figures

List of Tables

Nomenclature

∂	Partial differential
ANOVA	Analysis of variance
AFM	Atomic force microscopy
C	Concentration
CE	Counter electrode
CI	Confidence interval
CNT	Carbon nano tubes
CV	Cyclic voltammetry
CVD	Chemical vapour deposition
df	Degree of freedom
DMA	Dynamic mechanical analyzer
E	Modulus of elasticity
EC	Ethyl cellulose
gt	Grand total
HEPA	High Efficiency Particulate Arresting
HOPG	Highly oriented pyrolytic graphite
ITO	Indium tin oxide
MS	Mean squared
MSE	mean squared error
NNI	National Nanotechnology Initiative
PVA	Polyvinyl alcohol
RE	Reference electrode
rGO	Reduced graphene oxide
RL3	Risk level 3
Sc	correction for the mean
SE	Standard deviation
SEM	Scanning electron microscopy

S_p	Pooled variance
SS	Sum of the squared
STM	Scanning tunneling microscopy
T	temperature
TGA	Thermal gravimetric analysis
Var	Variance
XPS	X-ray photoelectron spectroscopy
WE	Working electrode
μ_k	Coefficient of kinetic friction

Chapter 1: Introduction

1.1 Graphene

Since 2004, when physicists, Konstantin Novoselov and Andre Geim, produced single-atom-thick crystallites from bulk graphite by micromechanical cleavage or the "Scotch tape technique", graphene has been drawing considerable attention among researchers because of its exceptional electronic and mechanical properties.

Graphene, as the building block of graphite, has a planar structure of sp^2 bonded atoms. The carbon atoms are structured in hexagonal lattice with molecule bond length of 0.142 nanometres.

The characteristics of pristine graphene have gone beyond the predicted theoretical limits. They have been proven by experiments conducted on single crystalline monolayer graphene. Setting outstanding optical and thermal properties of this material aside, the Young's modulus of 1 TPa and ultimate mechanical strength of 130 GPa are the highest values ever recorded [1, 2]. The inherent structure of graphene, with atoms in a 2D hexagonal lattice, would make it able to sustain extremely high electric current densities. These are the main reasons that have led to its nickname of "miracle material". These, however are the characteristics of pristine graphene without any structural defects which are highly difficult to achieve in the real world [2].

1.2 Motivation for Work

Graphene has been attracted much attention in scientific community because of its exceptional electronic and mechanical properties and its potential to be thermodynamically stable as a one atom layer thickness material [1, 2]. A wide range of research investigations have been conducted to properly quantify the properties of graphene. However, much of the work has used a single layer of graphene which presents three major problems: 1) The synthesis method for single layer graphene is not scalable as it requires significant resource inputs in both time and energy, 2) Single layer graphene is at nano-scale; therefore, it is not practically implementable in large scale applications. 3) The method by which large-scale graphene product has been made has imposed some restraints including geometry limitations. Although some advancements have been made on the production of large-scale single layer graphene by the chemical-vapor deposition (CVD) method, the resultant product tends to contain multiple structural flaws, resulting in a significant reduction in properties when compared with pristine graphene [3, 4].

Moreover, even if graphene offers theoretically superior mechanical properties, its electronic properties are gaining more interest in the last few years mainly because it can be produced as a flexible material, and the cost of the source material, which is carbon, is considerably less expensive in comparison with other competitors such as indium tin oxide (ITO) while delivering comparable features. Since its emergence, the electronics industry has been developing graphene for mainstream applications such as flexible batteries and supercapacitors.

Accordingly, the production of large scale graphene and a thorough understanding of its electrical and mechanical properties is crucial to properly exploit its potentials before it can be considered for potential applications in the field of flexible electronics.

1.3 Thesis outline

This thesis is divided into four chapters. Chapter one outlines the objectives and motivation for this work. Relevant research studies in the open literature on graphene properties and its synthesised methods are also provided in this chapter. Chapter two presents the methods used to prepare graphene powder. Moreover, this chapter provides the standard techniques and reference methods used to conduct the experiments. Chapter three presents the experimental results and addresses the challenges by proper statistical modeling and discussion. Chapter four provides concluding remarks. Also, it outlines the recommendations for future studies and works. Figure 1-1 is a flowchart to illustrate the how the experimental results are presented.

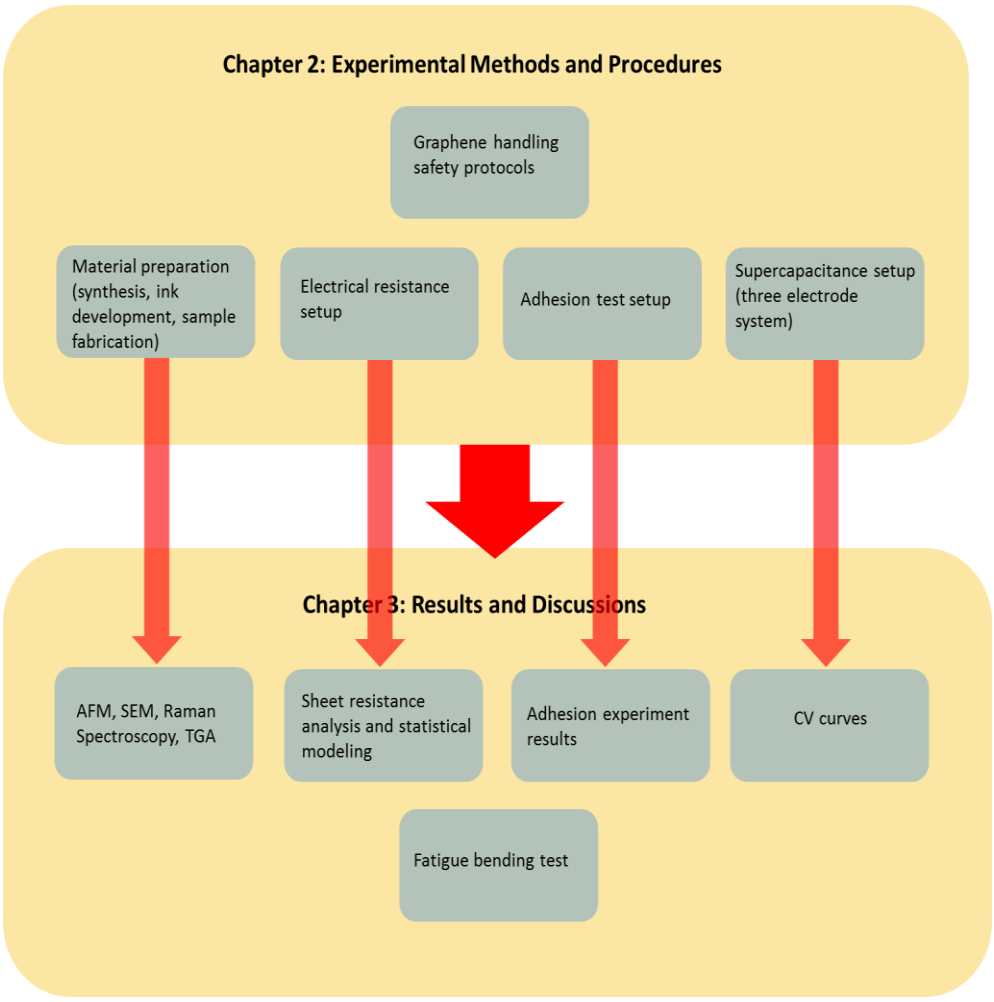

Figure 1-1 Experimental flowchart.

1.4 Review of Relevant Work

A review of the literature revealed a growing number of research papers on testing and characterizing of graphene products. Here, the most relevant research articles to provide background knowledge to develop methodology and experimental procedures for this work are reported.

1.4.1 Materials Synthesis

1.4.1.1 Introduction

Different methods have been developed to produce graphene from graphite, the most important of which are mechanical exfoliation, reduction of graphene oxide, chemical vapor deposition (CVD), and liquid-phase exfoliation [2, 5, 6].

1.4.1.2 Mechanical Exfoliation

Mechanical exfoliation of graphite includes peeling off graphene sheets from graphite flakes by introducing mechanical forces to overcome van der Waals attraction between adjacent graphite layers [7]. Micromechanical cleavage, also known as Scotch tape technique, is the primary method in this category which uses normal mechanical force to split layered graphite into graphene sheets [7, 8]. Lu et al (2010) [9], reported exfoliating of graphite flakes by manipulating atomic force microscopy (AFM) tip in which he created some highly oriented pyrolytic graphite (HOPG) regions and tried to carefully peel the graphene sheets off the graphite flakes by AFM tip.

Although mechanical exfoliation of graphite produces high quality graphene without any functionalized groups, the method is not sufficiently scalable, to produce the material volumes required for large scale applications.

1.4.1.3 Reduction of Graphene Oxide

Unlike the previous method which is based on mechanical processes, this method is mainly based on chemical processes. As the first step, graphite is processed into graphite oxide using strong oxidizing agents. Several methods exist mainly: Brodie (1860), Staudenmaier (1898), and Hummers (1958) [10]. Because of its hydrophilic nature due to oxygen functionalization, graphite oxide could be well-dispersed in water in large quantities. By using external power such as a sonicator, graphite oxide flakes can be separated into graphene oxide sheets which are hydrophilic as well. For this reason, although graphite oxide could also be dispersed in organic solvents, researchers have been using water as the main solvent at this stage [11, 12]. Finally, graphene oxide must be reduced by removing oxygen

groups. This could be done by various methods including thermal treatments and chemical processes. As a chemical treatment, graphene oxide could be reduced to graphene by using hydrazine, which is a strong reactive base and reducing agent. As a thermal treatment, it is reported that oxygen groups could be removed by heat treatment of graphene oxide at temperatures higher than 550 ˚C [13].

Although the method produces large amount of reduced graphene oxide (rGO), the quality of the resultant material is low mainly because of the attached functionalized groups.

1.4.1.4 Chemical Vapor Deposition (CVD)

Chemical vapor deposition of graphene includes depositing of reactive carbon based gases on a substrate. Different substrates such as Cu, Ni and Ru have been used for this method [14]. Generally, the substrate is pre-annealed up to high temperatures to increase its carbon solubility. After that, it is put in a reaction chamber while being exposed to carbon based gases such as methane. Gas molecules would decompose at the solid-gas interface; therefore, carbon atoms would dissolve into the substrate, forming a solid solution. As the final step, as the temperature goes down, the solubility of the substrate decreases and carbon atoms would form a graphene layer on the substrate.

Sukang Bae (2010) [15], has integrated the CVD method into roll-to-roll production and managed to produce 30 inch long graphene films.

Although the method could produce ultra-thin transparent graphene layers, it is particularly hazardous because of its gaseous by-products. Also, extremely high temperatures are needed for this process, which dramatically increases the cost of the process; this is not desirable for industry. Moreover, the resultant product would still have structural defects due to excessive concentration of grain boundaries as reported elsewhere [3, 4, 14].

1.4.1.5 Liquid-Phase Exfoliation

Liquid-phase exfoliation, also known as chemical exfoliation, of graphite includes splitting the graphite flakes into graphene sheets in a liquid media by introducing external forces provided by external devices such as a sonicator. Graphene dispersions could be prepared up to concentrations of 0.01 mg/ml by this method since the energy required to separate graphene flakes could be balanced by the solvent-graphene interaction provided a suitable solvent is used [16]. Though the quality of the graphite as the source material and the powder provided by the sonicator are contributing factors, using a solvent having a surface energy which matches that of graphene, has been shown to be the most significant factor in reaching high yield in liquid phase exfoliation [16, 17]. As well as producing high

quality graphene without introducing any functionalized groups, this method provides scalable amount of graphene in relatively short time. Therefore, due to its high quality non-functionalised graphene sheets, liquid phase exfoliation was selected as a proved high yield method.

1.4.1.6 Properties of Graphene Paper

Hierarchical solids are structures which contain sub-structural elements. This group of structures is classified based on their hierarchical order (n) indicating the level at which the structure is recognized. As a case in point, continuum solids are of a level n=0 or the first order of hierarchy which could represent a crystal with atomic lattice structure [18]. F. Barthelat (2006) [19], thoroughly examined the hierarchical structure of nacre. He demonstrated that the material is comprised of ceramic tablets arranged in columns and bonded together by a biopolymer. The specific Voronoi-like tiling [19] structure of ceramic tablets in this material gives it outstanding mechanical properties while having a light weight due to its organized internal structure.

The promising characteristics of the hierarchical structures and the need for large scale graphene, has lead the researchers to incorporate these ideas into graphene paper. Graphene paper is a highly organized structure, the building blocks of which are graphene sheets [20-23].

Haiqun Chen (2008) [20], has prepared graphene papers by vacuum filtration of aqueous dispersions of graphene sheets. The thickness of the papers was controlled by adjusting the volume of the colloidal dispersion. Also, he reported very conductive graphene papers with conductivities as high as 350 S/cm and strong mechanical properties in comparison with previously reported graphene oxide papers. The resulting material was also biomedically compatible for cell growth.

Yilun (2011) [21], has studied the mechanical properties of graphene papers with different cross-linking types. In a layer-by-layer assembly such as graphene paper, graphene sheets are bridged on the edges by intralayer covalent bonds and attached to each other by interlayer crosslinks. The van der Waals interaction between graphene sheets in interlayer crosslinks is considerably weaker. Therefore, it defines the failure mechanism of the structure. They classified different types of cross links based on chemical composition. Furthermore, they managed to derive their mechanical properties by numerical simulation and concluded that the mechanical properties of graphene papers highly depend on the cross link type.

Cristina Valles (2011) [22], prepared graphene papers by vacuum assisted flow filtration. She reported that annealing is a better way than chemical post process since it restores the pi-electron system

in graphene sheets and it provides enough thermal energy for graphene sheets to reorient in graphene paper for further electrical conductivity.

Guoqing Xin (2014) [23], reported large area free standing graphene paper fabrication by direct electro spray deposition of graphene dispersion integrated with roll to roll process. They sprayed the aqueous graphene solution on aluminum films. By immersing the films into the water, graphene paper peeled off due to different wetting angles between aluminum and graphene paper. The technique was able to achieve conductivities as high as 16000 S/m.

Zhe Weng (2011) [24], has integrated cellulose fibers in graphene paper for super capacitor applications. Using graphene based structure as the main material for electrodes, the cellulose fibers have been shown to be able to significantly improve electrolyte absorption and act as electrolyte reservoir to enhance ion transport between electrolyte and electrodes.

1.4.2 Mechanical Properties of Graphene

Changgu Lee et al. (2008) [1], have successfully obtained the mechanical properties of freestanding monolayer graphene, using nanoindentation in an atomic force microscope (AFM). They mechanically exfoliated the graphite flakes and deposited them on arrays of circular wells. Using AFM, the mechanical properties of monolayer graphene were probed by indenting the center of each graphene monolayer. They found from theoretical calculations that the Young's modulus was E = 1.0 TPa and intrinsic strength was 130 GPa for single layer graphene. Moreover, they demonstrated that the material undergoes a nonlinear stress-strain regime. The analysis yielded to the second- and third-order elastic stiffness of 340 N m^{-1} and −690 N m^{-1} respectively.

Research has been focusing on different mechanical properties of different types of graphene products (monolayer, bilayer, multilayer, graphene paper) in different applications such as additive manufacturing, flexible electronics, composite materials, energy storage and etc.

Vineet Dua et al. (2009) [25], are some of the pioneers in printing of graphene. They have successfully inkjet-printed graphene for sensor applications. Inkjet printing of graphene has been shown as a promising path in different applications ranging from storage systems to interconnects for electronic circuits. As a result, the mechanical properties of the interface between the printed patterns and the substrate have become significant, especially in flexible electronics applications.

Mingyuan Huang et al. (2009) [26], were among the first researchers to study the interface between a graphene monolayer and a flexible substrate by using Raman spectroscopy. They

demonstrated that the 2D and G bands exhibit red shift for monolayer graphene and G band splits into two distinct (G^+, G^-) features. Later on, researchers focused further on the interface of graphene and its substrate. By using in-situ Raman spectroscopy, they calibrated the strain induced by uniaxial loading, and found that monolayer graphene shows non-linear strain distribution in the direction of tensile axis as the strain of the substrate increases uniformly [27].

L. Gong et al. (2010) [28], have studied the interfacial stress transfer in graphene monolayer nanocomposite. Having intact flake-matrix interface during load transfer as the underlying assumption, they modeled the behaviour of a discontinuous flake in a matrix using shear-lag theory and proved that the fundamental concepts of continuum mechanics are still valid in that scale. They not only managed to accurately estimate the maximum shear stress, but also derived the shear stress distribution at the interface. Their work was further developed by others until Tao Jiang et al. (2014) managed to derive the equations for the shear stress transfer using non-linear shear lag theory considering interfacial sliding [29].

Research on the mechanical properties of graphene has focused beyond elastic properties.

I.A. Ovid'ko (2013) [30], has published a thorough review on the effect of structural defects on mechanical properties of graphene. It was said that the plastic deformation and fracture of graphene is significantly influenced by the presence of defects in the lattice structure. There are different types of defects experimentally observed in graphene lattice structure, the two most important of which are dislocations and grain boundaries. Dislocations are point defects which violate the perfect hexagonal lattice structure of graphene. They represent pentagon-haptagon pairs in the 2D hexagonal crystal lattice. Plastic deformation mostly happens through the motion of lattice dislocations. On the other hand, grain boundaries are the line defects separating graphene grains with different crystal lattice orientations. It is mentioned that the grain boundaries and out of plane ripples decrease the strength of graphene by order of magnitudes.

The mechanical characterization of the miracle material has been on-going.

Peng Zhang et al. (2014) [31], managed to quantify the fracture toughness of graphene. In the field of material science, the fracture toughness is a property that describes the ability of a material containing a crack to resist fracture. The fracture toughness of graphene was measured as the critical stress intensity factor of $4 \pm 0.6\, Mpa\sqrt{m}$. Using experiments and molecular dynamics simulations, they verified the applicability of the classic Griffith theory of brittle fracture to graphene.

Seung-Mo lee et al. (2015) [3], published a review on common defects in graphene produced by chemical vapor deposition (CVD). They presented several effective methods to detect those defects in early stages or to overcome them as the last step. According to this review, the second law of thermodynamics (maximizing entropy) explains the presence of defects in crystalline materials. The dangling carbon bonds induced by structural imperfections has been provided as one of the most significant reasons that the fracture properties of graphene are below expectations as they react with other molecules such as H_2O, H_2, O_2 and etc. These adsorbents have dramatic effects on the structural properties of graphene and create new physical-chemical properties. Atomic resolution scanning tunneling microscopy (STM) was suggested as an effective method to diagnose these effects in early stages of CVD. A healing process was also presented, accomplished by exposing the vacancies by CO, NO gas. The CO gas would place in the vacancies, and a NO molecule would remove the extra O by forming NO_2.

1.4.3 Electrical Properties of Graphene

The exceptional electronic properties of graphene were the primary reason that the material has gained considerable interest in recent years. Therefore, it is useful to provide to brief overview of some fundamental aspects related to the electronic properties of graphene.

Inversion symmetry is solely responsible for the unique electronic properties of graphene. This includes: 1) planar 2D structure, 2) honeycomb lattice structure, and 3) having identical atoms in all of the lattice sites [32]. There are two different bonds in graphene structure: 1) strong in plane covalent bonds, also known as σ bonds and 2) valence bonds, also known as occupied π bonds.

Three of the four valence electrons are used by σ bonds in each carbon atom to connect to its three nearest neighbours, creating a strong hexagonal planar structure. Carbon atoms are separated by 1.42 Å and the angle between them is 120°. The fourth valence electron occupies the $2p_z$ orbitals which are perpendicular to the hexagonal lattice plane. When half-filled $2p_z$ orbitals from adjacent carbon atoms overlap, π bonds would be made. These bonds are primarily responsible for the charge transport in graphene. Figure 1-2 demonstrates the configuration of different bonds on graphene.

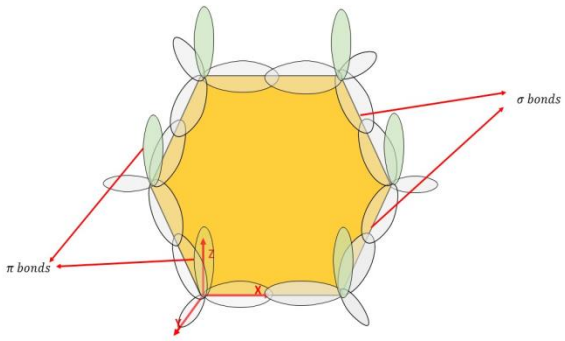

Figure 1-2 Illustration of $\boldsymbol{\sigma}$ and $\boldsymbol{\pi}$ bonds on graphene monocrystalline.

Single layer graphene is known for its outstanding electronic properties because of its theoretically defect- free lattice structure. However, the material structure would be more disordered as the graphene layers stack up even if each individual graphene sheet is a perfect crystal. This would shorten carrier mean free path; hence, reducing electrical conductivity [33]. Needless to say, the existence of impurities or introducing functionalized groups could increase interlayer spacing which alters the perfect structure of the material, hence reducing the electrical conductivity.

The electrical properties of graphene products are highly dependent on the way by which graphene sheets are stacked, number of graphene layers , type of structural defects, concentration of lattice disorders and supporting substrate, while the method by which graphene sheets has been synthesised is equally critical .Consequently, it is not accurate to merely classify the sheet resistance of graphene products based on the method by which their graphene has been synthesised [4, 34, 35].

Sukanta De (2010) [4], reported that many graphene products do not have the minimum electronic requirement to be used in flexible electronic application. Due to its relatively low production costs, graphene could be a viable solution for flexible electronic industry especially since carbon nano tubes (CNT) fell short of being a promising candidate because of its high production costs(1600 $/g). However, indium tin oxide (ITO) is currently used as the main material for this application with sheet resistance as low as 10 Ω. Therefore, any potential alternative must at least meet this requirement. Graphene produced by CVD was suggested as a potential replacement for ITO due to its transparency and flexibility, yet its relatively high sheet resistance limits its implementation. Substrate-induced doping of graphene was proposed as a viable solution. It was mentioned that substrate usually diminishes the electronic properties of graphene; therefore, certain amount of doping should be

achieved to compensate this loss. It was shown that graphene could be n doped to the standard requirement if coated with a thin layer of polyvinyl alcohol (PVA).

K.I. Bolotin (2008) [33], reported the presence of impurity scattering as a major barrier in limiting carrier transport capability of graphene by shortening carrier mean free path to less than a micron. He achieved carrier mobilities in excess of 200,000 $cm^2 V^{-1} s^{-1}$ at electron densities of 2×10^{11} cm^{-2} by suspending single layer of graphene on Si/SiO_2 substrate. Also, a considerable direct improvement in mobility enhancement for unsuspended samples was reported by cleaning the surface from impurities by introducing large current through the device.

H. Castro Neto et al. (2009) [36], have widely examined the electronic properties of a single layer and multilayer graphene. He demonstrated that the material is a unique system in many ways and its electronic properties are controlled mostly by Dirac fermions. They also presented that different types of disorders modify the Dirac equation leading to unusual spectroscopic and transport properties. However, as was correctly mentioned in that paper, they just studied pure carbon structure. Chemical modification of graphene or introducing functionalized groups or different dopings could entirely change the electronic properties of this material.

1.5 Objectives and Scope of Work

The main objective of this research study is to investigate the feasibility of developing electrically conductive and highly structured "graphene paper" by depositing multilayers of graphene ink onto substrates. To achieve this objective, the scope of work included:

- Synthesis of graphene powder using a scalable technique that would not considerably deteriorate the properties of pristine graphene,
- Developing stable graphene ink, using appropriate solvents, which is both able to contain high concentrations of graphene and having the appropriate viscosity for large scale graphene deposition,
- Conducting sheet resistance tests to determine the dominant factors that affect the resistivity of the graphene paper and representing this property with a mathematical model,
- Investigating a set of relevant mechanical properties for flexible electronics application, and
- Characterizing the material using standard characterization techniques such as AFM and SEM.

Chapter 2: Experimental Methods

2.1 Introduction

This chapter presents the experimental work conducted to synthesize graphene/ethyl cellulose (EC) powder and ink. It is followed by the design and description of the techniques used to fabricate graphene paper samples, measure electrical resistance, study the adhesion of graphene paper to its substrate and investigates the capacitance behaviour of the material.

For flexible electronic applications, the most important characteristic of graphene products is their electrical properties. Therefore, having a strong understanding of the electrical resistance value and fundamental charge carrier transport mechanism is crucial to properly exploit the properties of this material [4, 37, 38]. Also, the suggested materials for flexible electronic application should retain their electrical properties after repeated mechanical loads in order to have predictable functionality [37-40]. Moreover, flexible supercapacitor components are inseparable part of modern flexible electronic circuits [2, 24, 37, 41]. For practical implementation, the capacitance behaviour of the produced graphene paper was determined as part of our feasibility study.

2.2 Graphene/ Ethyl Cellulose (EC) Powder Synthesis

The procedure used to obtain graphene powder is based on a liquid exfoliation technique published earlier and is known to be successfully adopted to produce different graphene products [38]. First, 10 g natural graphite flakes (3061 grade, Asbury Graphite mills, Absury, USA) and 2 g ethyl cellulose (EC) (EC: Aldrich, viscosity 4 cP, 5% in toluene/ethanol 80:20, 48% ethoxy) are added to 200 ml ethanol to obtain a stable graphene dispersion.

The mixture is then ultra-sonicated (B2500A-DTH, Ultrasonics Cleaner, VWR North American, Burlington, ON, Canada) for 6 hours to separate the graphite flakes, reducing the number of the sheets in each graphite flake. To prevent overheating the flammable solvent, the mixture is suspended in an ice bath which is replenished every 40 minutes. Sedimenting the thick graphite flakes at the end of the sonication process, the desired liquid on top of the solid residue (also known as the supernatant) is then collected and transferred into 200 ml centrifuge tubes.

To further filter the liquid media from graphitic flakes, ultra-sonication is followed by centrifuging (Sorvall™ Legend™ X1 Centrifuge Series, Thermo Scientific™). This separates the desired material which remains suspended in the liquid from the thick flakes which stick to the tube walls. The supernatant is then removed from the tubes and diluted 4:1 with ethanol by volume. An aqueous solution of NaCl (99.5%, EMSUR®, Denmark) (0.04 g/ml) is then added to the diluted liquid suspension in a 2:1 ratio to both remove the extra solvent and EC in the dispersion and to flocculate graphene/EC particles. These are then separated by centrifuging for 8 minutes at 10000 g and decanting the water/solvent residue from the centrifuge tubes. At this point, the desired particles are separated out of the liquid and are stuck to the centrifuge tube walls. Finally, the particles are re-dispersed in ethanol, and the whole centrifugal purification process repeated to ensure that the large graphitic flakes are removed from the dispersion and only graphene/EC particles are retained in the sediment.

In order to ensure no salt/solvent residue remains, the bottles are filled with deionized water to wash the solid. This also allows the flocculated graphene/EC particles to be peeled from the tube walls and dispersed in the water. Afterwards, the dispersions are vacuum-filtered (0.45 μm filter paper, Nylon, HNWP, Millipore) to collect the particles. Finally, the filters are air dried for 10 hours allowing a dark grey graphene-EC powder to be obtained by scraping the particles (shown in Figure 2-1) [42]. Based on the SEM characterization done previously, the approximate graphene sheet size is 300 nm as demonstrated in Figure 2-2 [42].

Figure 2-1 Dark grey graphene/EC powder [Reprinted with permission of Elsevier] [41].

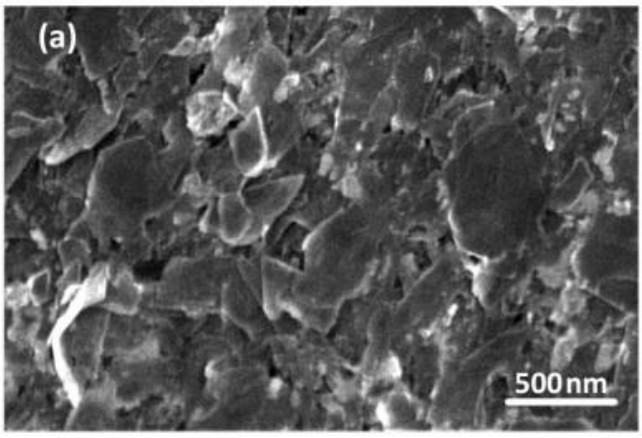

Figure 2-2 SEM picture demonstrating the approximate graphene sheet size [Reprinted with permission of Elsevier] [41].

2.3 Ink Development

Cyclohexanane and terpineol solvent blends are used since they have been widely recognised for their capability to dissolve high concentrations of graphene and the blend viscosity can be readily modified to suit the needs for printing application [43, 44]. First, a stable homogenous ink is prepared using 0.3 g graphene/EC powder, 7.5 ml cyclohexanane and 1.5 ml terpineol. Although the viscosity of the ink had been adjusted for the printing application reported in [38, 42], it resulted in "coffee ring" effect when drop casting contentious film samples. Therefore, the viscosity of the ink was increased by using 3 ml terpineol instead of 1.5 ml, totally eliminating the coffee ring effect. Figure 2-3 shows the graphene ink obtained.

Figure 2-3 Stable graphene

2.3.1 Validation of Chemical Composition

To ensure that the fully annealed dispersion of the graphene/EC powder ink has more of a graphene structure rather than any other carbon product, X-ray photoelectron spectroscopy (XPS) was previously conducted on the fully annealed dispersion of graphene/EC powder ink specimens synthesized using the same method [42].

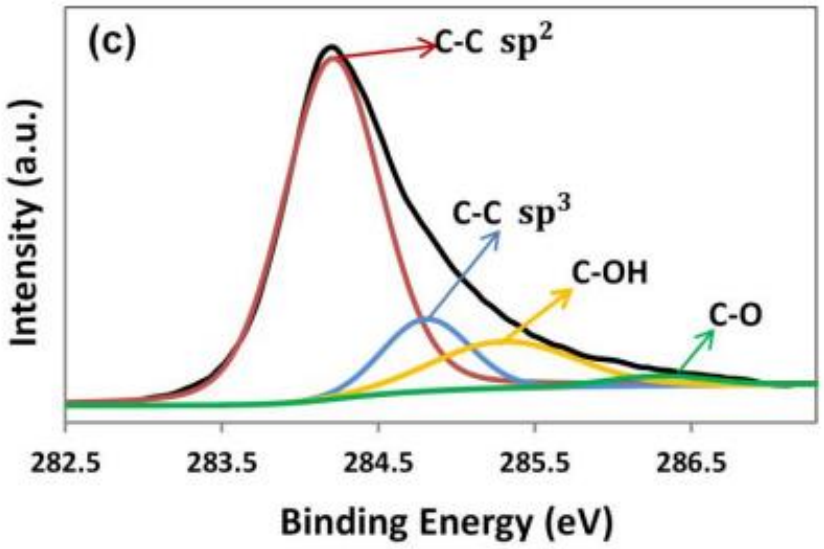

Figure 2-4 XPS result conducted on fully annealed dispersion of the graphene/EC powder ink [Reprinted with permission of Elsevier] [41].

The results of the XPS are provided in Figure 2-4 [42], showing that the intensity of C—C sp^2 peak is by far higher than any other peaks, which verifies that the product is closely related to graphene.

2.4 Sample Preparation and Fabrication

2.4.1 Introduction

Different depositing methods for applying graphene ink have been developed since graphene was discovered. The primary methods producing consistent results can be categorized in two ways: 1) printing; and 2) Meyer Rod method.

2.4.1.1 Printing

Ink jet printing of graphene ink has been increasing in popularity because it produces desirable patterns with a high level of consistency. Other printing methods such as aerosol-jet printing have been used in recent years to print micro interconnects, but are less prevalent [42].

At the heart of an inkjet printer, there are many nozzles which act as orifice plates. As illustrated in Figure 2-5, they eject the ink out while the print head is scanning the printing area. In most of the inkjet printers, the ink is ejected by thermal technology. In each print head, small heaters are located over the channels leading to each nozzle. By heating the ink, a bubble is created building up pressure and forcing the ink out. When the bubble collapses, more ink is sucked into the channel.

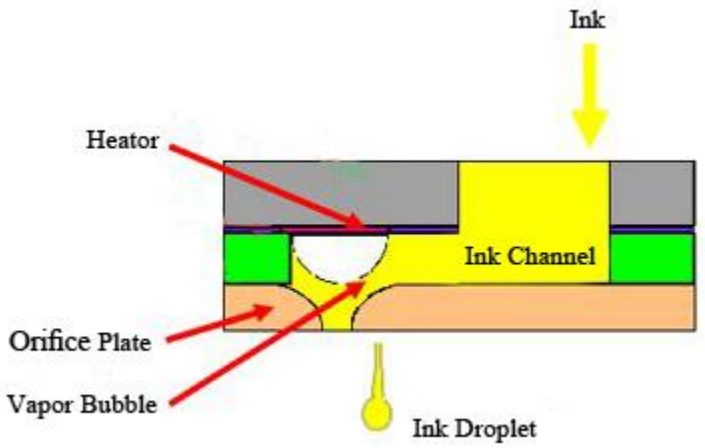

Figure 2-5 Inkjet printing mechanism [Reprinted with permission of IS&T: The Society for Imaging Science and Technology sole copyright owners of www.imaging.org].

Inkjet printing of graphene has both advantages and disadvantages. The main advantage of inkjet printing is that it can produce desirable patterns in a very controlled manner in a relatively short time. However, the use of graphene in industry would require large scale graphene deposition and its characterization; the inkjet printing is therefore not an optimal solution. This is because graphene ink should be filtered to select the particles before using in inkjet printer, i.e., a large number of graphene nano sheets would be disposed of since they simply do not have the required size to pass through the

nozzles. This does not favor large scale deposition. Therefore, inkjet printing was not selected as the deposition method in this work.

2.4.1.2 Meyer Rod Method

Also known as the metering rod, this method has been a well-known scalable coating technique in thin film coating industry since it can be used in roll-to-roll production and could produce uniform and continuous large scale coatings in a very controlled manner [40, 45, 46].

As shown in Figure 2-6, a Meyer Rod is a metal bar wound tightly by a wire in different diameters. The grooves between the wire coils and the viscosity of liquid media determine the thickness of coating that will pass through as the rod moves along the surface.

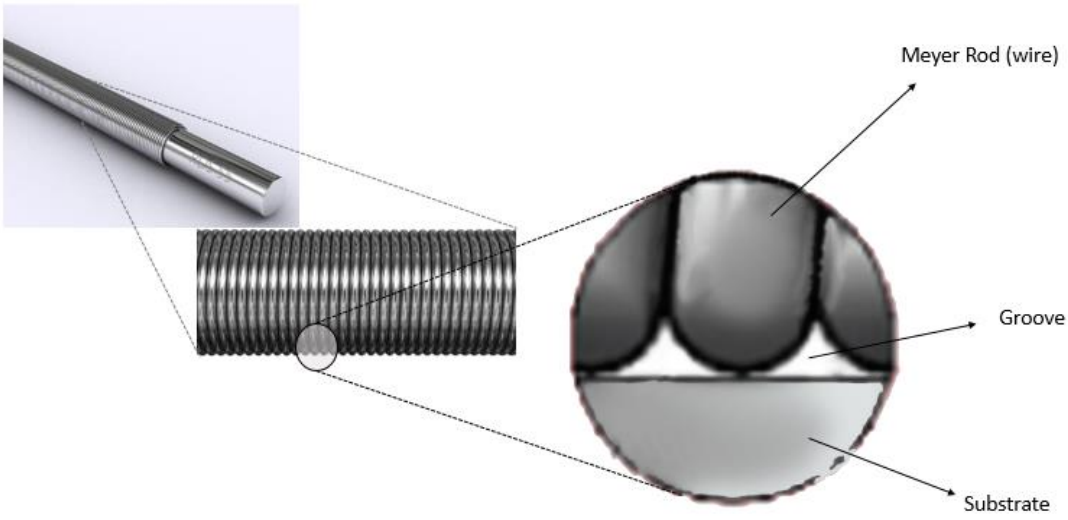

Figure 2-6 Illustration of Meyer Rod.

Due to its recognised characteristics in large scale film coatings, the Meyer rod method has been used for large scale graphene deposition as well. Jie Wang (2012) [40], reported using the Meyer rod for large scale fabrication of uniform graphene coatings. Coatings with different thicknesses were achieved by adapting the concentration of graphene dispersion and using rods with different wire diameters.

It is possible, using the Meyer rod method, to achieve large scale uniform coatings with reasonable control over the thickness mainly because no particle size selection was needed; hence, no

material loss. In this work, however the desired coating thickness could not be achieved to fabricate specimens for electrical resistance experiments or mechanical experiments. Therefore, the Meyer rod method was not suitable in this work either.

Through experimental trials, it was found that graphene ink could spread and produce a scalable, uniform and thick enough coating by carefully adjusting the viscosity of the ink in drop casting process. Hence, the drop casting was eventually selected as the deposition method to produce samples required for this study.

2.4.2 Experimental Setup

The polyimide film commercially known as Kapton was used as the substrate for the experiments since it is both flexible and thermally stable over a wide range of temperatures [47]. Also, it is widely used as the substrate in flexible electronics applications [38, 48]. Before deposition, the kapton films were carefully cleaned by ethanol. After that, 1.5 ml of ink was drop-cast on the surface. It was observed that a 1.5 ml of graphene ink would have sufficiently large numbers of graphene nano platelets to cause them to stack up on each other and deposit continuous graphene paper as a hierarchical structure. With the adjusted viscosity, the deposited drops would spread out uniformly and air-dried in 60 minutes leaving a uniform large scale graphene/EC paper on the surface without any coffee ring effect as shown in Figure 2-7. As demonstrated in Figure 2-8, the relatively large graphene/EC paper is then cut into various geometries using a paper cutter and placed inside a furnace for post-process annealing to remove EC and leave behind graphene paper on kapton.

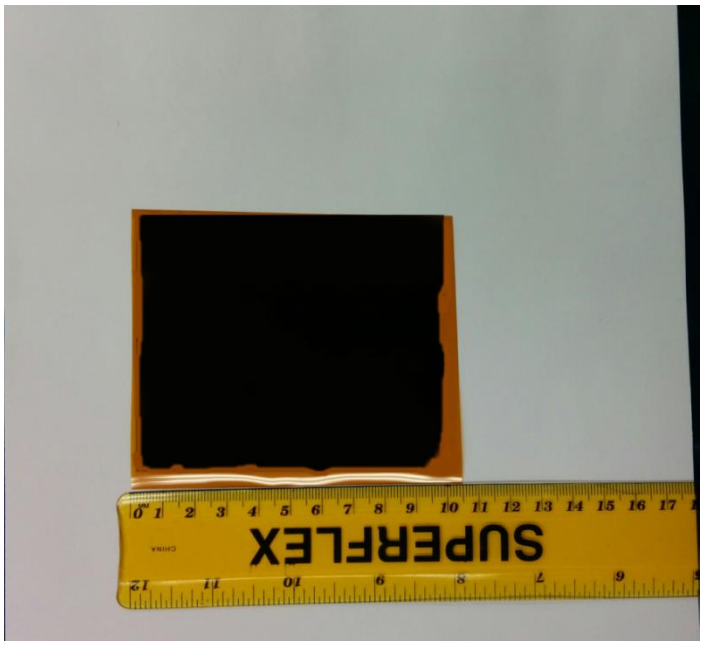

Figure 2-7 Large scale graphene/EC paper deposition on Kapton.

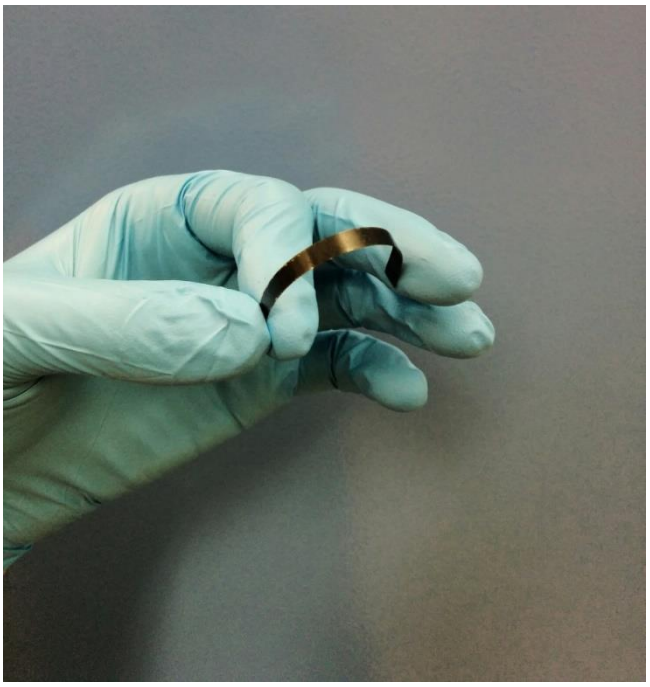

Figure 2-8 Graphene paper samples cut in rectangular strips.

2.5 Graphene Handling Safety Protocols

2.5.1 Introduction

Nanotechnology has been experiencing promising advancements for diverse applications ranging from bioengineering to composite materials since it emerged [2, 49]. Considering the huge potential impact in all the sectors of economy, the US established National Nanotechnology Initiative (NNI) in 2001 to explore the opportunities that nanotechnology could provide.

The carbon nanotube (CNT) is a well-known example of carbon nano products. The exceptional electronic and mechanical properties of CNT have been considered as a paradigm change for nanotechnology in 21st century [49, 50]. The physicochemical properties of this material have been shown to enhance the performance of many industrial products. However, the generally proven success of CNT in other fields has not offered the same utility in biocompatible applications such as medicine [49-51]. Stefano Bellucci (2009) [50], reported that 400 μg/ml of oxidized multi-walled CNTs could result in massive loss of T cells through programmed cell death, while pristine CNTs were comparatively less toxic. Xingchen Zhao (2011) [51], published a thorough review on nano-toxicology of CNTs on organism, organ, cell, and biomacromolecule levels. The importance of particle size was mentioned as the major reason for several unpredicted neurological problems such as translocation of inhaled nanoparticles to the brain through the olfactory neuronal pathway which has not been reported from previous studies on large particles. Also, other health problem issues including suppression of systemic immune function, oxidative stress and an increase of dermal cell number were reported on small mammals such as rats when exposed to sufficient dosage of CNT through skin contact and lung inhalation.

When considering graphene platelets, it should not be surprising that the toughest material ever discovered are also potential health related hazards based on the findings on nano-based CNT. Ken-Hsuan Liao (2011) [52], studied the cytotoxicity of graphene oxide and graphene on human red blood cells and skin fibroblasts. The study indicates that red blood cell membranes could be disrupted by the strong electro static interactions between graphene platelets and phosphatidylcholine lipids existing on the outer surface of red blood cells. However, this damage is completely dose dependent. According to this study, the concentration of graphene sheets leading to 50% lysis of red blood cells is more than 200 μg/ml.

As a result, adherence to safety measures in this study is crucial in all the stages from synthesis of the nano powder to working with solidified ink on the substrate.

2.5.2 University of Waterloo Nano Material Regulations and Handling Procedure

According to the University of Waterloo safety office website, the material in the form of nano powder is classified as Risk level 3 (RL3). To minimize the risk of exposure, these materials must always be handled inside a glovebox (Figure 2-9) with minimum criteria as below [53]:

- HEPA filter on outlet
- Antechamber to allow for a secondary protection when moving product into and out of the glovebox.
- Made of a material composition that is compatible to the materials being used in the glovebox (namely solvents)
- Must exhaust to outside if being used with a chemical that poses a secondary hazard like a flammable or toxic solvent.

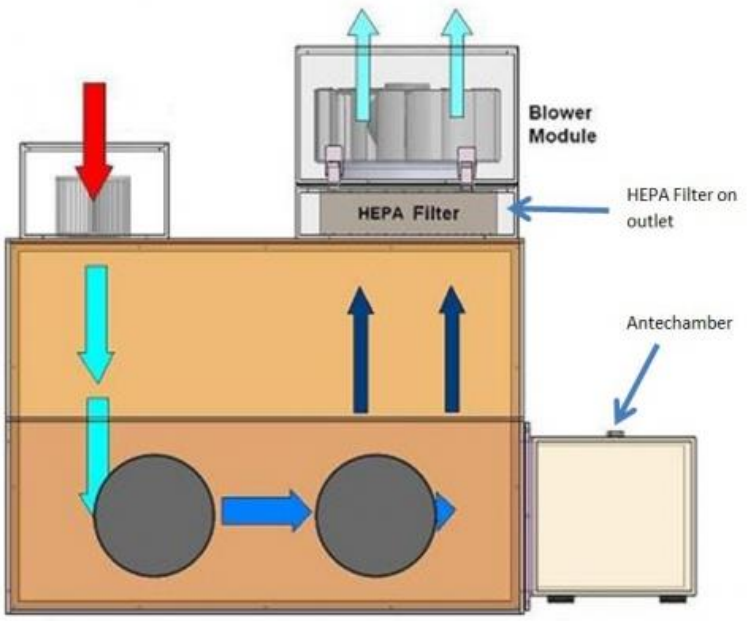

Figure 2-9 Illustration of a HEPA filtered glove box. Image courtesy of Cleatech, Cleanroom and Laboratory Solutions.

Therefore, the process of air drying the wet filter papers and scraping off the graphene/EC powder from the papers were conducted inside the glovebox. As it was not possible to inject solvent inside the glovebox, the amount of required powder was carefully weighed on a scale inside the glovebox and then placed inside a vial. Then, a septa was rolled over the vials inside the glovebox for the solvent to be injected afterwards as shown in Figure 2-10.

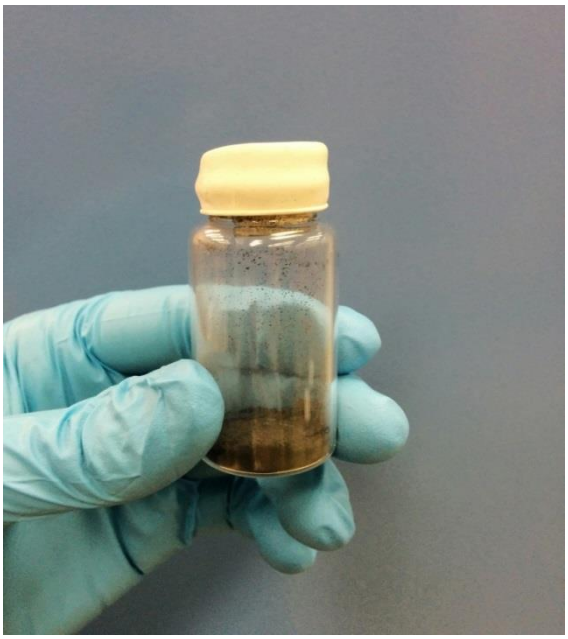

Figure 2-10 Graphene/EC powder vial with a rolled over septa.

According to the University of Waterloo safety office website, when nano materials are inside a liquid media or bounded in a solid matrix, they are relatively safe and could be handled on a bench top or a typical fume hood since they do not pose the same aerosolization risk.

Therefore, after the solvent was injected inside the vials through septa, the resultant mixture is expected to be safe to handle in a standard laboratory environment both in liquid form and after the annealing process.

2.6 Electrical Resistance Measurements

2.6.1 Introduction

For an electrically conductive material, electrical resistance is a property indicating how difficult it is for electrical current to pass through the material. By definition, the electrical resistance of a material (R) is proportional to the ratio of the voltage (V) across it to the electrical current (I) through it.

$$R \propto \frac{V}{I} \rightarrow \ R = K\frac{V}{I} \ (K = proportionality\ constant) \qquad \textbf{Eq 2-1}$$

For a wide range of materials, K equals to 1. This is called Ohm's law, and the materials satisfying this condition are called Ohmic materials.

The resistance of a given material is primarily a function of two variables: 1) what the material is made out of; and 2) its shape or geometry. That is, the resistance is inversely proportional to the material cross section and directly proportional to its length, given the electrical field is linear all through the length of the sample. Therefore for a material with constant cross section:

$$R = \frac{\rho\ l}{A} \qquad \textbf{Eq 2-2}$$

where R is the electrical resistance measured in ohm (Ω), l is the length measured in meter (m), A is the cross section area measured in square meters (m^2) and ρ is the electrical resistivity measured in ohm-metres ($\Omega \cdot m$).

For rectangular samples with constant thickness and width:

$$R = \frac{\rho\ l}{A} = \frac{\rho\ l}{Dt} \longrightarrow \frac{RD}{l} = \frac{\rho}{t} = R_{Sheet\ Resistance} \qquad \textbf{Eq 2-3}$$

where D and t are width and thickness of the samples respectively.

Four point probes are the instruments which are commonly used for resistance measurements. However, the direction of the electric field lines is non-linear since the probes must be perpendicular to the conductive material, so it does not create a regular linear electric field. As a result, an appropriate

mathematical formula for electrical resistance is needed. We first consider a general expression for a resistance measurement device with equal probe spacing [54]:

$$R = \frac{\rho}{2\pi sF} \qquad \textbf{Eq 2-4}$$

where R is the electrical resistance measured in ohm (Ω), ρ is the electrical resistivity measured in ohm-metres ($\Omega.m$), s is probe spacing measured in meter (m), F is the correction factor for location near sample edges.

In the present work, a custom-built electrical resistance device was used for the following reasons:

- In-situ resistance measurements were necessary for some experiments. Since the standard four point probe instrument is heavy and not portable.
- An electrical fixture ensuring linear electric filed lines would simplify the math considerably; hence, it would save a lot of time and energy.

2.6.2 Experimental Setup

In this study, an electrical fixture was built, as schematically shown in Figure 2-11 to obtain an electrical field that would be linear and with minimal errors when testing the graphene paper samples. The copper bars were pressed into the acrylic base and resistance measurements were done by a two points probe voltmeter attached to the copper bars.

Rectangular graphene paper samples 5 mm in width and 20 mm in length were fabricated. To ensure that full contact is achieved between the rectangular samples and copper bars, a microscope slide with 50 g weight on top was used to provide a known contact force, Figure 2-12. The electrical resistance of the samples was then measured by a two point probe voltmeter attached to the copper bars. The sheet resistance of the samples was then calculated by multiplying the electrical resistance by a factor of 0.25, i.e., the width-to-length ratio. Figure 2-13 shows the entire device set-up.

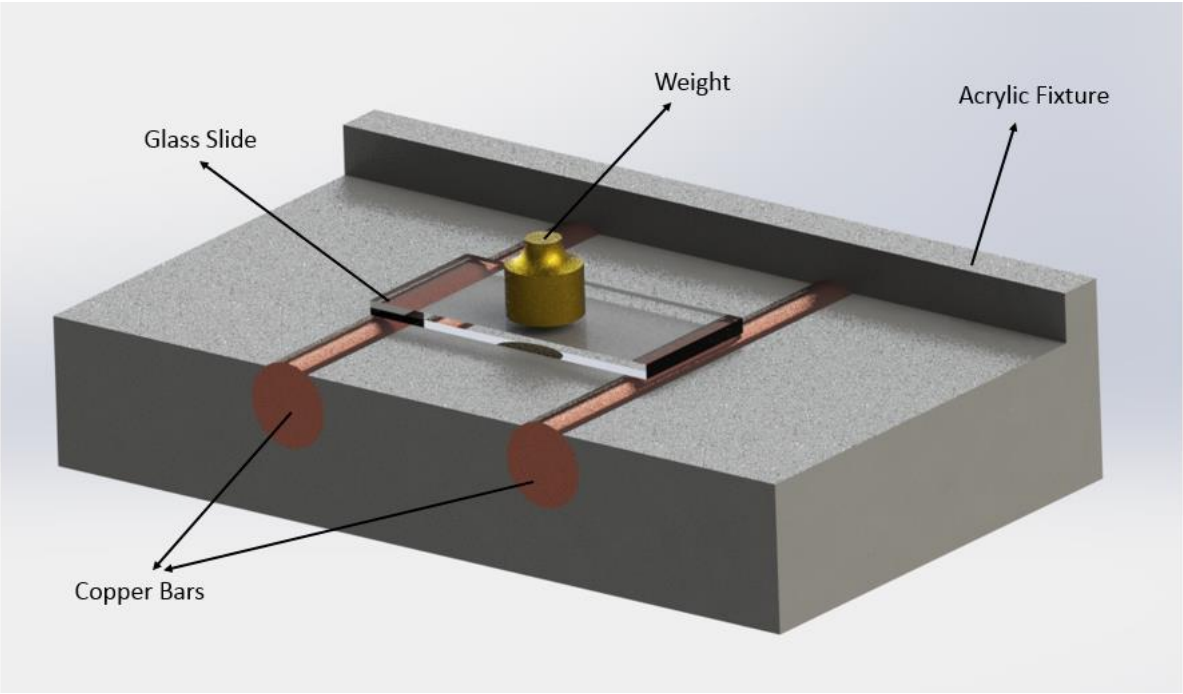

Figure 2-11 3D representation of the electrical fixture and its components.

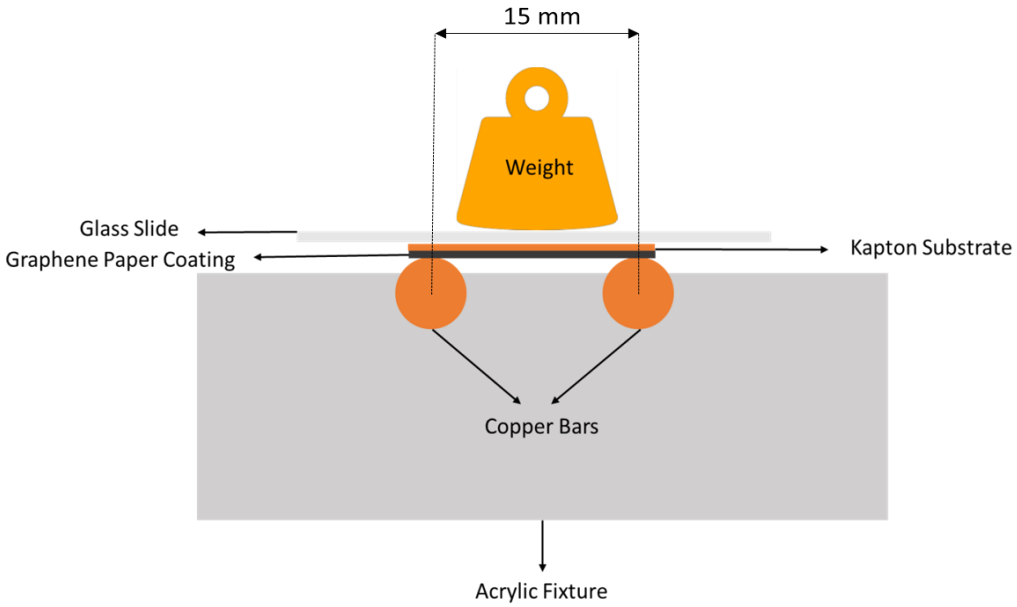

Figure 2-12 2D representation of the electrical fixture and its components.

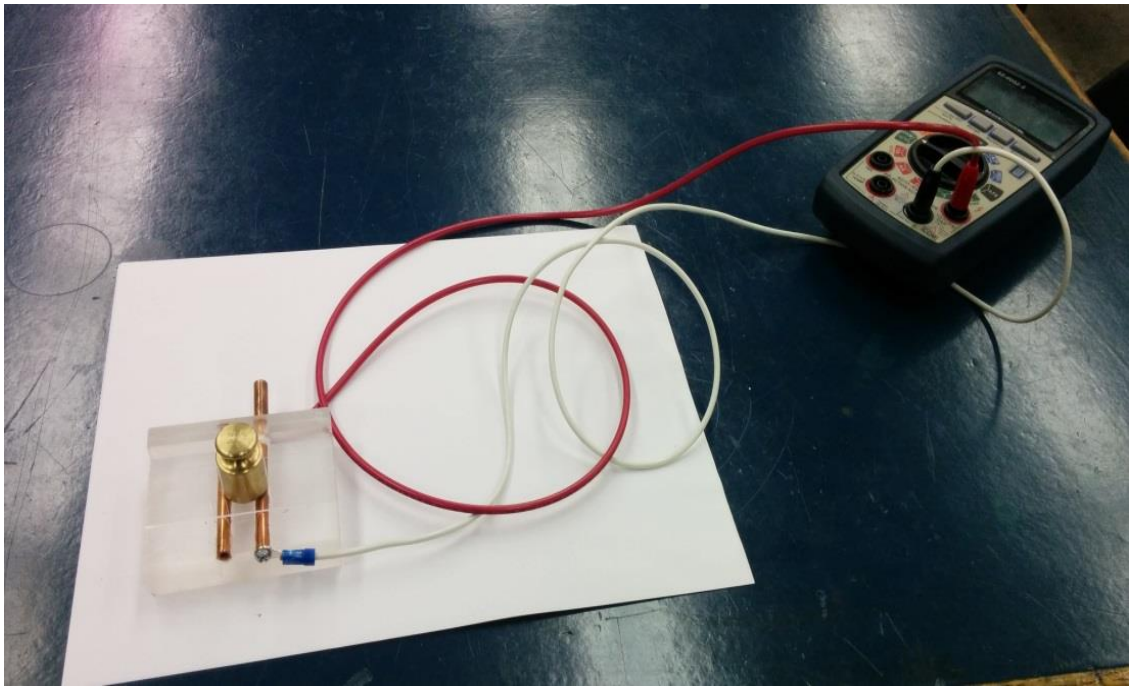

Figure 2-13 The electrical fixture attached to two points probe voltmeter.

2.7 Adhesion test

2.7.1 Introduction

Qualitatively speaking, adhesion means how strongly two similar or dissimilar materials are stuck together. Quantitatively speaking, it is more difficult to consider a unique definition for adhesion; therefore, researchers classify it in three different forms: 1) basic adhesion, 2) thermodynamic or reversible adhesion, and 3) experimental or practical adhesion.

Basic Adhesion: it explains the nature and strength of the forces sticking two materials which are in contact with each other. The examples of these forces could be ionic strength, covalent forces and etc.

Thermodynamic or Reversible adhesion: The reversible work done to create a unit area of the interface between two materials. This is not practical for our application as there are various unknown parameters.

Experimental or practical adhesion: there are two different ways in measuring this type of adhesion: 1) in terms of maximum force per unit area required to practically separate two materials 2) in terms of work required per unit area to detach two materials. The mathematical relationship between these two is as follows where W is the work of adhesion and $f(x)$ is the force of adhesion:

$$W = \int f(x)dx \qquad \textbf{Eq 2-5}$$

In experimental adhesion, if the break precisely occurs at the interface of the thin film and the substrate, it is called adhesive failure. If the break occurs through the thin film media, it is called cohesive failure representing the weakest plane in the system. Measured experimentally may be quite different from estimated theoretically from the mechanisms described above.

The current work is interested in characterising the adhesion between the graphene layer and the kapton substrate. While there are a number of tests for determining the adhesion of two layers. In this work, the lap shear test is chosen [34]. This test has been used for characterizing thin film adhesion properties which includes coatings [34].

We assume that the graphene paper can be represented as a thin film coating. As will be seen later in Chapter 3, this assumption is verified by atomic force microscopy. Regardless of their

application, the mechanical and electronic characteristics of thin film coatings all depend on their adhesion to their supporting substrate. Below are the primary reasons for the significance of the adhesion of the thin films to the substrate.

- The durability and longevity of thin film devices is primarily dependent on the adhesion. For example, in electronic circuits.
- Kinetics of film structure growth are significantly influenced by adhesion. Material crystals would grow wherever the cohesional energy exceeds the adhesion energy, which determines the performance of the film.

There are different methods of measurement of adhesion of thin films such as qualitative methods, non-destructive methods, mechanical methods, practical methods and etc. However, a mechanical method is most appropriate since it would provide relevant data in terms of flexible electronics applications which is a potential use of graphene paper.

According to [34], mechanical methods could be categorized into two different classifications according to the direction of the force applied to the film by the method: 1) methods involving normal force to fully/partially detach the film from the substrate; and 2) methods involving lateral force to fully/partially detach the film from the substrate.

In applications of flexible electronics, such as wearable devices, the large curvature of the devices results in shear as the predominant failure mode especially when there are multiple thin layers. We therefore studied the shear behaviour of graphene paper coating using the lap shear method. Tangential shear or lap shear method, which is a standard adhesion test involving lateral force, was selected for this study since the electrical resistance change due to shear force is most likely failure mode in service applications.

2.7.2 Experimental Setup

In order to conduct adhesion test experiments, a type of setup which is both capable of accurately measuring the force and adjusting the force acting on the sample was required. For this purpose, the setup shown in Figure 2-14 was prepared. The setup comprised a load cell on a horizontal platform with a film gripper at one end and an electronic chip controlling the load cell at the other end. The electronic chip controls the load cell such that it always pulls the sample with constant velocity regardless of the amount of the force being applied. As schematically shown in Figure 2-15, samples

were mounted on the film gripper while they had a backing underneath. Then, a layer of soft tissue, Kimwipe, was placed on the sample. Different weights were placed on the tissue and retained with the help of a retort stand holding a rubber ring. Therefore, friction force was applied on the surface of the graphene paper by the surface of the tissue when the sample as being pulled by the load cell. Finally, the desired results were recorded by visually checking the tissue for residue and reading the force value displayed on the load cell.

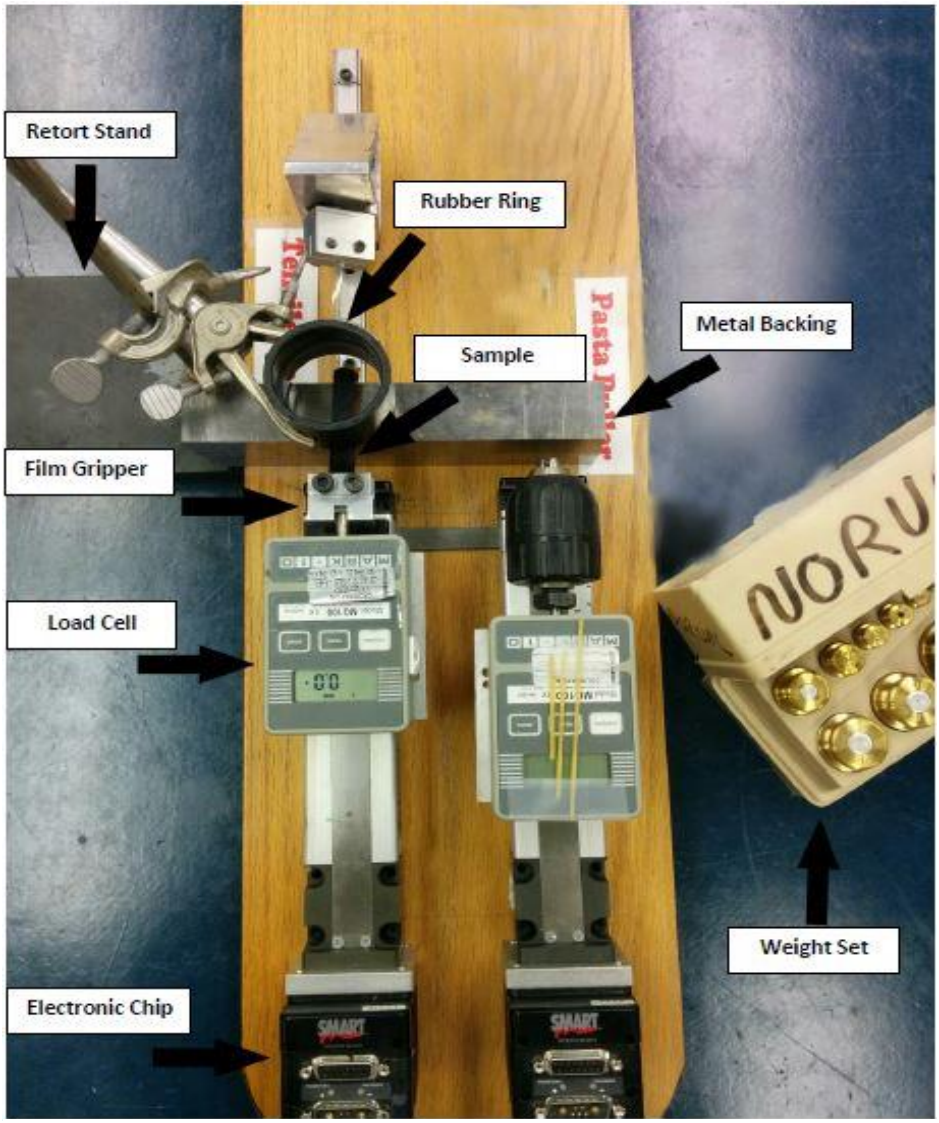

Figure 2-14 Adhesion test setup and its components.

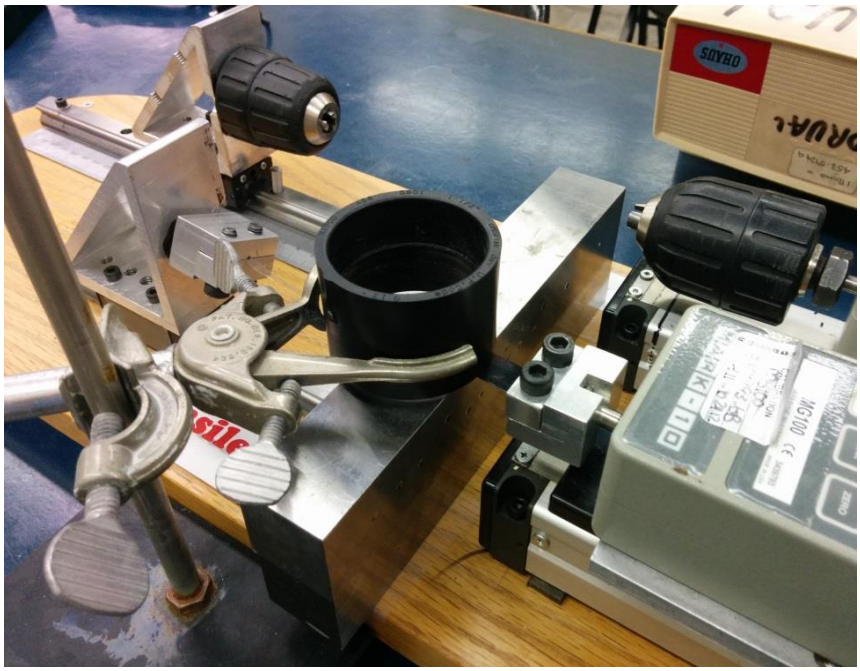

Figure 2-15 Adhesion test setup and its components.

2.8 Supercapacitance Test

2.8.1 Introduction

Batteries as the standard storage units in electronic devices cannot meet the power requirements for many applications. Therefore, considering a separate pulse power device, also known as capacitor, is becoming more significant. Since traditional capacitors used in electronic circuits could not provide enough pulse energy for some applications, researchers have been developing high-energy-density capacitors, also known as ultacapacitors or electrochemical capacitors, to meet this demand. The advantages of supercapacitors over pulse batteries are their high power capability, efficiency and long shelf life which make them an attractive alternative. However, their low energy density compared to batteries limits them to applications in which relatively small quantities of energy is required [41].

Figure 2-16 demonstrates the basic structure of a supercapacitor. It consists of two electrodes immersed in an electrolyte which are separated by a separator. Electrodes are fabricated from a metal acting as a current collector which is coated by high surface area, porous material with the pores in nanometer range, also known as the active material. The role of current collector is to collect electrical current for the device for maximum performance, while the role of active material is to provide numerous reaction sites for electrolyte ions to be able to store energy electrochemically in the pores or at the interface between solid material and liquid electrolyte. It is convenient to categorise the storage mechanisms in supercapacitors as double-layer and pseudo-capacitance processes separately. In this work, we will only focus on double-layer capacitors [41].

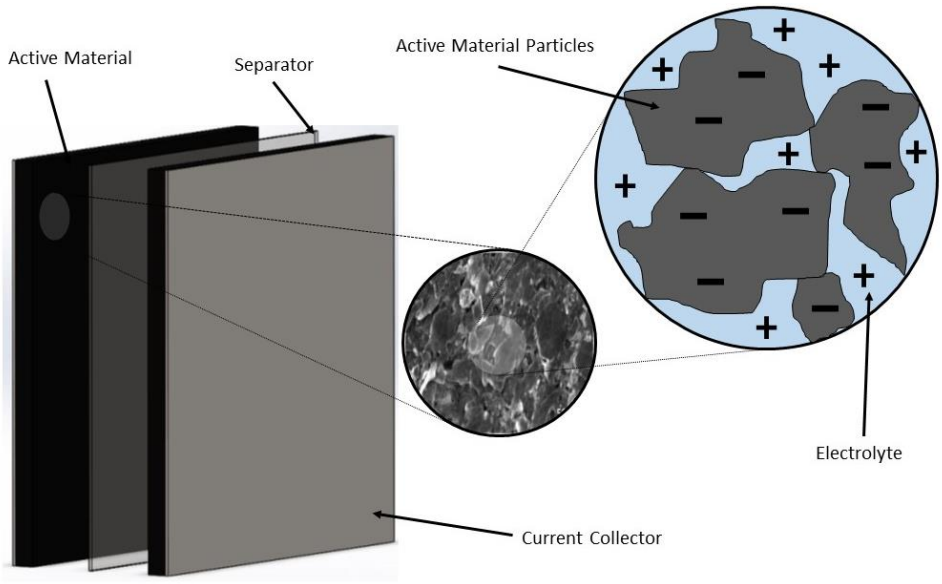

Figure 2-16 Basic structure of a supercapacitor.

2.8.1.1 Double Layer Capacitors

The charge separation in the form of double layer formation is the main storage mechanism in double layer capacitors. As mentioned above, this occurs in the micropores or at the interface between the solid electrode and the liquid electrolyte. The characteristics of the active material such as surface area and pore size distribution are the key factors that determine the capacitance.

Activated carbon is one of the popular materials which are used as the active material for supercapacitors. It is mixed with a binder such as ethanol to make a slurry to be rolled on the electrode with controlled thickness. The thickness of the electrode is generally in the range of 100-300 microns with 65-80% porosity. It should be also noted that the large fraction of pores in carbon materials could

not be accessed by electrolyte ions since they are too small. This is specifically true for organic electrolytes. This explains why aqueous electrolytes are preferred for carbon supercapacitors since the size of the ions are much smaller in comparison with organic electrolytes [41].

Over the past few years, researchers have been integrating advanced carbon materials such as CNT or graphene into supercapacitor technology. Yu (2010) [55], reported the production of ultra-thin, transparent and conductive graphene layers by CVD. She used the material both as the current collector and active material for her electrodes. Tao (2013) [56], reported high performance transparent all solid state supercapacitors by integrating CNT into a conductive binder functioning both as the electrode and active material.

2.8.2 Experimental Setup

As shown in Figure 2-17, electrodes have been made by using Ni as the current collector and graphene paper coating as the active material. After that, the electrodes were heated at 300 ^{o}C and 500 ^{o}C for 40 minutes to degrade EC and cure the graphene paper [57].

Figure 2-17 Ni/Graphene electrode for supercapacitance test.

Supercapacitance experiments were conducted by using a standard three electrode system (Biologic Potentio Sta, VSP 300) with SCE reference electrode and platinum as counter electrode. 2 molar KOH was used as aqueous electrolyte. The voltage range was selected between 0-1 V with 20 mV/s as voltage rate. Figure 2-18 illustrates a schematic of the three electrode system used for this test.

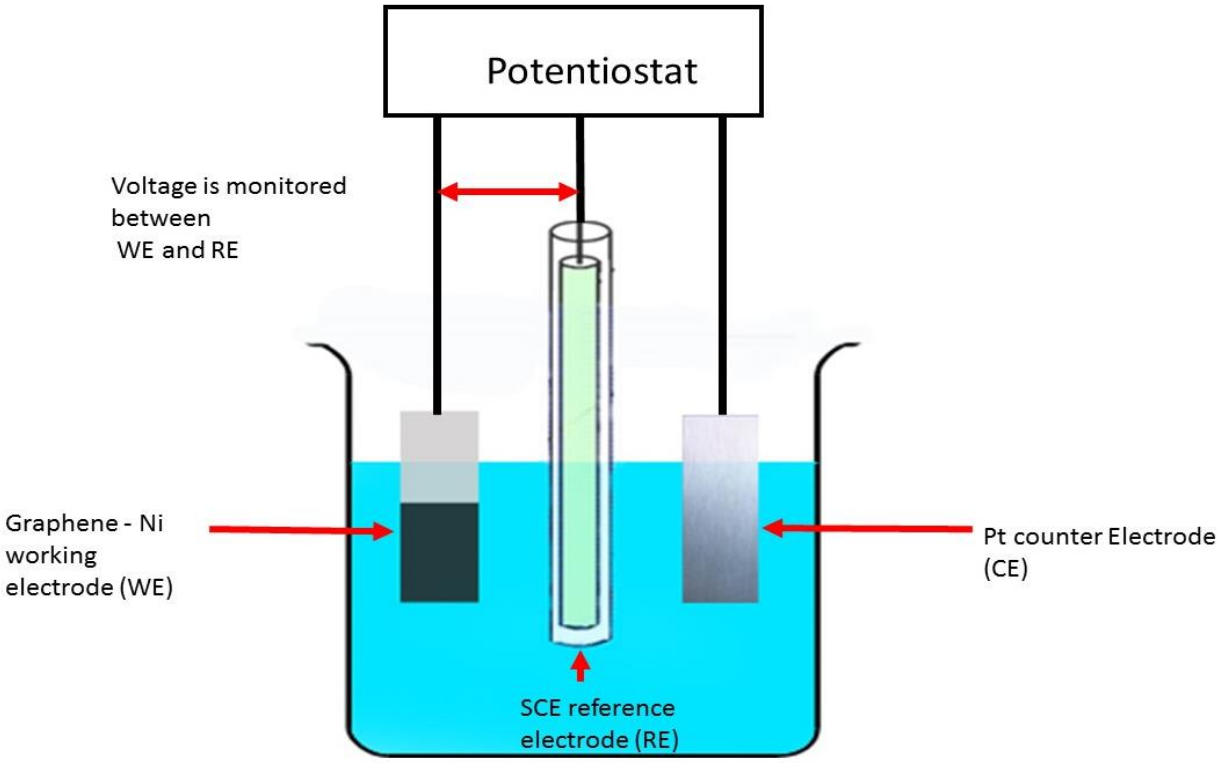

Figure 2-18 Three electrode system schematic.

In total eight electrodes were prepared and tested, including three at 300 ^{o}C and five at 500 ^{o}C. The former temperature was selected to align with other sheet resistance tests while the higher temperature is expected to cause complete degradation of EC.

Chapter 3: Results and Discussion

3.1 Introduction

This chapter will present and discuss the experimental results. First, the electrical resistance of graphene paper is modeled as a function of different variables. Results for mechanical testing related to cyclic bending, adhesion and strength properties are then presented. As further characterization, Raman spectroscopy has been conducted to determine phase purity. Finally, cyclic voltammetry tests were used to investigate capacitance behavior of synthesized graphene paper.

3.2 Graphene Paper Thickness

The thickness of graphene paper is needed to calculate its electrical resistivity as per Eq 2-3. Atomic force microscope (AFM) (BRUKER, Innova®, USA) in tapping mode with Nanoscope Analysis software was used to determine the approximate thickness of graphene paper films. Figure 3-1 and Figure 3-2 demonstrate typical thickness measurements of two different samples with 3 mg/ml powder concentration annealed for two hours and four hours, respectively, at 300 ^{o}C. Figure 3-3 demonstrates thickness measurements of a sample with 1 mg/ml powder concentration annealed for two hours at 300 ^{o}C. Using the edges, the thickness of graphene paper coating was independently measured with AFM using kapton film as the baseline. As an approximation, the average thickness read off from the thickness histogram of the 3 mg/ml samples was taken to be 200 nm (Figure 3-1 and Figure 3-2). For the 1mg/ml sample, the approximate average thickness was estimated at 90 nm (Figure 3-3).

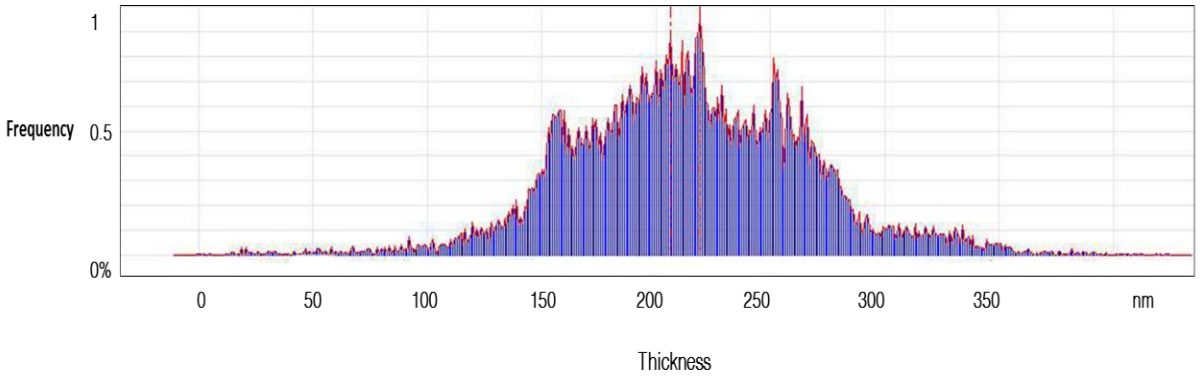

Figure 3-1 AFM measurement for with 3 mg/ml concentration annealed at 300 ^{o}C for two hours.

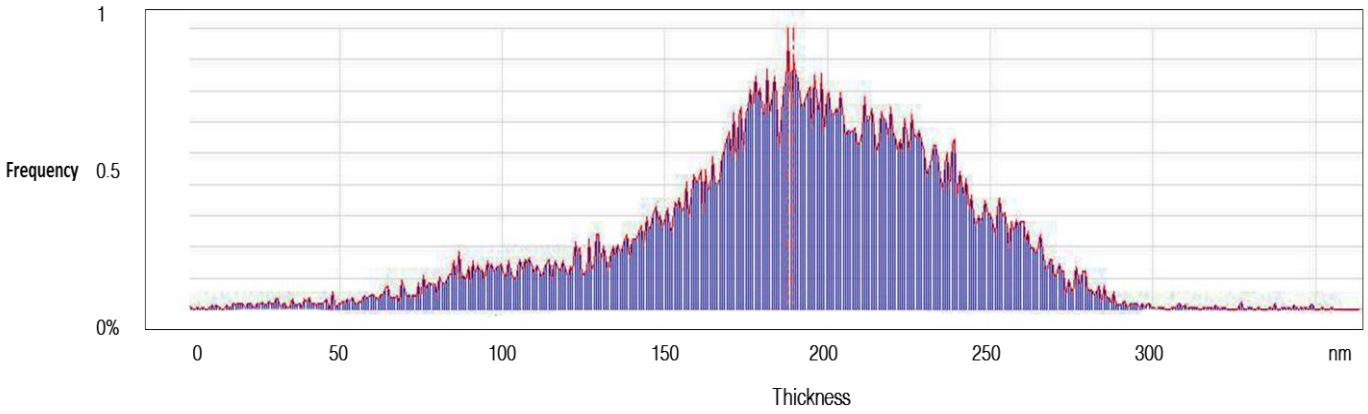

Figure 3-2 AFM measurement for with 3 mg/ml concentration annealed at 300 ^{o}C for four hours.

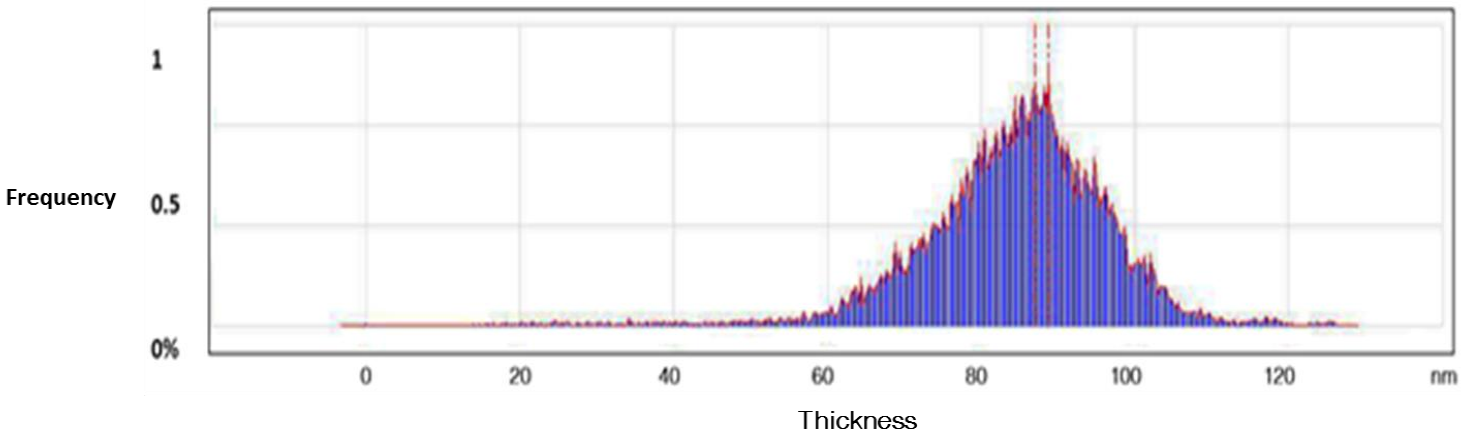

Figure 3-3 AFM measurement for with 1 mg/ml concentration annealed at 300 ^{o}C for two hours.

3.3 Sheet Resistance Analysis

Eq 2-1 expression can be used to estimate the instrument error as follows:

3.3.1 Instrument Error Estimate

Differentiating the resistance expression,

$$R = \frac{\rho l}{A} = \frac{\rho l}{Dt} \qquad \textbf{Eq } 2\text{-}1$$

$$y = f\,(x, y, z, \dots) \longrightarrow\; df \cong \left|\frac{\partial f}{\partial x}\right| dx + \left|\frac{\partial f}{\partial y}\right| dy + \left|\frac{\partial f}{\partial z}\right| dz + \cdots \qquad \textbf{Eq 3-1}$$

where dx, dy and dz represent the error acting on x, y and z variables.

$$dR = \left|\frac{l}{Dt}\right| d\rho + \left|\frac{\rho}{Dt}\right| dl + \left|\frac{\rho l}{t}\right| \frac{dD}{D^2} + \left|\frac{\rho l}{D}\right| \frac{dt}{t^2}$$

and by assuming that the resistivity of the sample is constant along the length, gives:

$$\frac{dR}{R} = \frac{\left|\frac{\rho}{Dt}\right| dl + \left|\frac{\rho l}{t}\right| \frac{dD}{D^2} + \left|\frac{\rho l}{D}\right| \frac{dt}{t^2}}{\frac{\rho l}{Dt}} \longrightarrow \frac{dR}{R} = \frac{dl}{l} + \frac{dD}{D} + \frac{dt}{t}$$

It is known that if the resolution of an instrument is considered as Δx, its error is $dx = \Delta x/2$.

Samples were fabricated with constant width of 5mm (0.005 m). The width of the samples was measured by micrometer. Therefore, $dD = \frac{10^{-6}}{2}$.

Thickness of the graphene paper was approximately obtained from atomic force microscopy (AFM) to be around 200 nm. Therefore: $dt = \frac{10^{-9}}{2}$.

$\frac{dD}{D} + \frac{dt}{t}$ would be almost zero based on the values provided above. Therefore: $\frac{dR}{R} \cong \frac{dl}{l}$

The length over which the electrical current passes through the sample is constant for all the samples since the distance between copper bars does not vary and is 15 mm. As a result, for $\frac{dR}{R}$ to be around 10%, $dl \cong 1.5\ mm$.

Since the distance between the copper bars is constant, the above condition implies that samples should be mounted on the fixture with their sides parallel to the sides of the fixture to make sure $dl \cong$

$1.5\ mm$ is indeed the error limit. As a short stopper is built at the end of the fixture and by using a microscope slide to flatten the samples as much as possible during measurements, it is reasonable to assume that the variance on the measurements due to instrumental errors is much lower than 10%.

3.3.2 Experiment Results and Modeling

Graphene products are considered to have predictable and temperature dependent electrical behaviour [20, 38, 58]. Although all the graphene paper samples have been annealed at 300 ^{o}C in this work, they showed better or comparable electrical behaviour to the values previously reported for graphene paper annealed at the 1000 ^{o}C temperature range [20-23]. The lower annealing temperature is great advantage that dramatically decreases the cost of the production.

Five different annealing times [40 mins, 2 hrs, 4 hrs, 8 hrs and 24 hrs] were selected as the explanatory variables to investigate the effect of the annealing time on the sheet resistance. With three different independent replicates for each experimental condition, fifteen graphene paper samples with 3 mg/ml powder concentration were prepared and annealed at 300 ^{o}C to ensure that the annealing process is repeatable and the error estimates for the experimental process would be sufficiently accurate. Figure 3-4 illustrates a sample fabricated for this experiment.

Figure 3-4 Graphene paper sample for electrical resistance experiment.

Table 3-1 Experimental data acquired for sheet resistance analysis.

Sample name	Sample name	Sample name	Annealing Time (hrs)	R1($k\Omega$)	R2($k\Omega$)	R3($k\Omega$)
271115-S012RA	11215-S013RA	11215-S014RA	0.75	2.54	2.74	2.74
271115-S022RA	11215-S023RA	11215-S024RA	2	2.24	1.88	1.71
271115-S032RA	11215-S033RA	11215-S034RA	4	1.4	1.4	1.62
11215-S042RA	21215-S043RA	21215-S044RA	8	0.98	1.04	0.97
11215-S052RA	21215-S053RA	21215-S054RA	24	0.19	0.15	0.16

Eq 3-2 is used to model this electrical resistance behavior, and the confidence interval curves for resistance values were derived based on ANOVA analysis.

$$R = Aln(t) + B \qquad \textbf{Eq 3-2}$$

where R is the sheet resistance measured in kilo ohm ($k\Omega$), t is the annealing time measured in hours, $A = -0.72 \pm 0.06$ and $B = 2.46 \pm 0.12$. Moreover,the value for $R^2 = 0.98$ for this regression analysis which is an excellent representation as shown in Figure 3-5, where lower and upper CI indicate lower and upper confidence intervals, respectively.

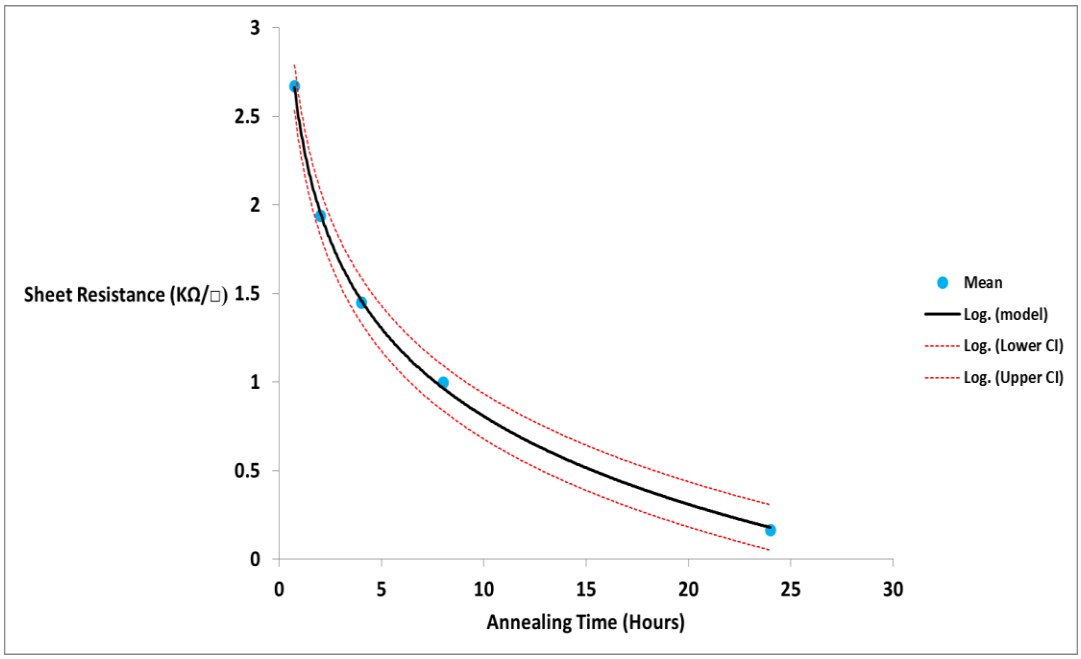

Figure 3-5 Sheet resistance vs annealing time plot.

As seen in Figure 3-5, it was possible to achieve a sheet resistance as low as 150 ohm from nonconductive graphene/EC paper. It is thus highly likely that the thickness of the coating changes as the annealing time increases; therefore, samples with different annealing times were measured for the thickness by AFM. According to the AFM measurements, it is reasonable to say that the thickness of the samples is around 150-300 nm. As a result:

$$R_{Sheet\ resistance} = \frac{\rho}{t} \longrightarrow \rho = R_{Sheet\ resistance} \times t \longrightarrow \quad \textbf{Eq 3-3}$$

resulting in:

$\rho = 140 \times 300 \times 10^{-9} = 42 \times 10^{-6}\ ohm.m$

To the author's best knowledge, this resistivity is better or comparable to the best results reported for graphene papers and other graphene products [20, 22, 23, 38, 42, 57-59].

As shown in Figure 3-5, the sheet resistance of graphene paper logarithmically drops with annealing time. This can be attributed to the reduction in d-spacing in the lattice structure of graphene papers as previously reported [20, 22, 60], which would enable mobile charges to travel along the structure more easily [20, 33]. Moreover, the excessive thermal energy provided by longer annealing time would allow graphene nano platelets to reorient and restore the pi-electron system which eventually recovers the electrical properties. However, this mechanism may not occur in our process as their annealing temperature is 700 ^{o}C, while our annealing temperature is 300 ^{o}C [22].

It should be noted that the concentration of graphene in graphene/EC powder is less than 10% [42]. However, reported graphene papers in the literature have used aqueous rGO (see nomenclature) dispersions to make graphene paper, which causes most of their structure to be made out of graphene nano platelets without any polymer stabilizer. The graphene paper, however, is reported to have higher resistivity [20-23]. This could be due to the presence of EC (see nomenclature), which is a polysaccharide. Figure 3-6 illustrates the chemical composition of EC. It is known that the glass transition temperature of EC is about 130 ^{o}C, its melting point is around 180 ^{o}C and and its decomposition temperature is around 300 ^{o}C [61]. The working temperature for this experiment was set to be 300 ^{o}C which is well above the melting point. Figure 3-7 demonstrates thermal gravimetric analysis (TGA) on graphene/EC powder in air. It could be seen that the powder begins losing its mass at about 200 ^{o}C. The powder loses up to 90% of its mass when the temperature reaches 400 ^{o}C. This could be attributed to the decomposition of EC [42, 62]. It is widely known that sugar like molecules

could be burnt by oxygen and produce CO, CO_2 and H_2O. Since the samples were annealed in the furnace with air flow, a similar chemical reaction is expected. On the other hand, the annealing temperature used for the graphene paper samples in this experiment is 300 ^{o}C. According to the TGA scan in Figure 3-7, only 40% of the EC mass decomposed at this temperature. Therefore, the rest of EC mass still remains as liquid polymer between graphene platelets. This could allow graphene nano flakes to move and get in contact with each other, providing the essential electrical path for the electrical current to pass through. Another possible mechanism for electrical conductivity could be the char left behind by EC burning. X. Li (1999) [62], reported that EC could produce less than 10 wt% char yield when it burns. Therefore, low quality carbon chars could act as connections between graphene nano platelets providing an improved electrical network for the electrical current to pass through.

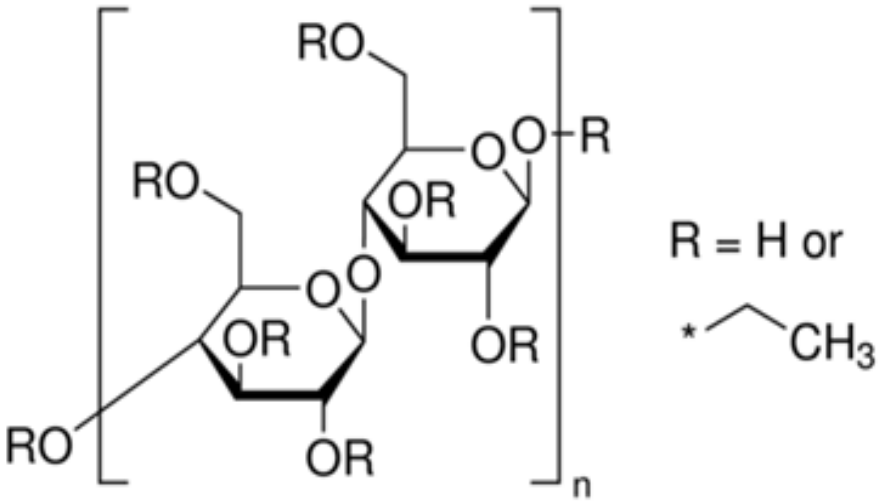

Figure 3-6 Chemical composition of EC used for this experiment [Courtesy of Aldrich® Chemistry].

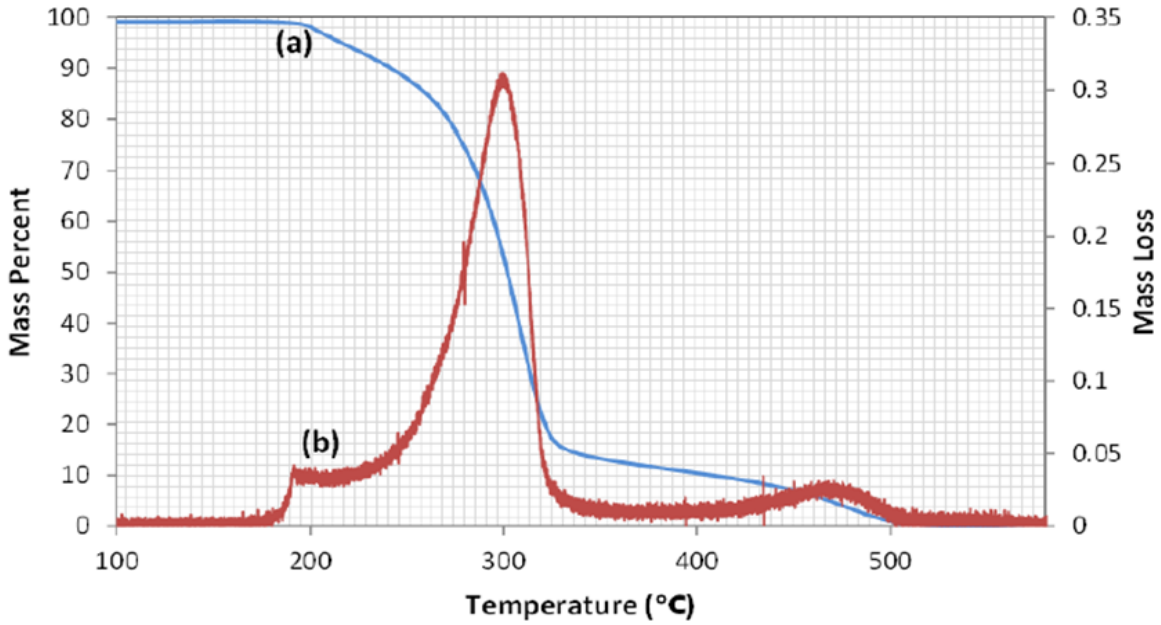

Figure 3-7 TGA analysis on graphene/EC powder showing (a) mass changes versus temperature (left axis) and (b) the differential mass loss (right axis) [Reprinted with permission of Elsevier] [41].

It is useful to understand why the conductivity of the present samples outperforms most other graphene paper products. One reason could be ascribed to the dense and packed structure of our samples. Other graphene paper has been produced by vacuum filtration of colloidal dispersions of rGO. Although a mechanical press was used to make the structure much denser [23], the electrical resistance between deposited layers could degrade the electrical properties of the paper considerably. That is, charge carriers would be provided with branched electrical paths in different directions, which is one of the main reasons for low electrical properties of graphene products. Furthermore, the quality of graphene-sheet-graphene-sheet connection in our paper samples could be better due to all the aforementioned reasons. Also, rGO has been widely known for its low quality nano platelets because of its residual attached functionalized groups. In contrast, our results suggest highly conductive minimally functionalized nano platelets as the building block of the hierarchical structure of graphene paper. This hypothesis will be verified later via Raman spectroscopy. Also, most of the graphene papers reported have been annealed at high temperatures (700 ^{o}C - 1000 ^{o}C) to remove their oxygen content as much as possible. This could also have detrimental effects on the internal properties of graphene nano platelets.

3.4 Modeling of Electrical Sheet Resistance

Having a solid quantitative understanding of the electrical properties of graphene paper is crucial to properly exploit its properties in electronic applications. The conductivity of graphene products has been widely studied in the past as a function of single variables such as density of the as-prepared solution/ink or annealing temperature [20, 23]. However, there is still a lack of accurate statistical models obtained from experimental data which can account for the main contributing factors and their interactions. We offer here a fully replicated full factorial design (2^k, k=3) with multiple duplicate measurements at each level to determine the significant experimental factors and their interactions on the sheet resistance measured in this work. That is, at each corner of the design space, different samples were fabricated and randomly put in different furnaces as independent replicates. For comparison, different samples have been fabricated and put in the same Pyrex dish inside the same furnace as duplicate measurements. The design window in which the experiments have been conducted is as follows:

Temperature=[280, 320] ^oC, Time=[2, 4] hours and Concentration=[1, 3] mg/ml. Table 3-2 demonstrates the results acquired from this experiment. It should be noted that the value for each cell represents the average of the duplicate measurements; however, each cell is an independent replicate.

Table 3-2 Experimental data acquired for sheet resistance modeling.

A=Temp (C°)	B=Time (hrs)	C=Concentration (mg/ml)	R1($k\Omega$)	R2($k\Omega$)	R3($k\Omega$)
280	2	1	8.46	5.17	8.37
280	2	3	1.28	1.40	1.79
280	4	1	1.79	2.50	3.77
280	4	3	1.14	1.11	1.20
320	2	1	3.05	3.00	3.54
320	2	3	0.97	0.86	1.00
320	4	1	1.46	1.14	1.25
320	4	3	0.94	0.26	0.17

In this experiment, annealing temperature, annealing time and concentration of the as prepared ink were considered as the main contributing factors. As the first step, the sheet resistance of the samples were measured as the y values. In order to minimize the correlation between the parameters, an orthogonal design is used. In other words, all the upper and lower limits of the design variables (T,t

and C) have been changed to +1 and -1 respectively.Table 3-3 demonstrates the orthogonal full factorial design for this experiment.

Table 3-3 orthogonal full factorial design for sheet resistance modeling experiment.

A=Temp (C°)	B=Time (hrs)	C=Concentration (mg/ml)	AB	AC	BC	ABC	R1($k\Omega$)	R2($k\Omega$)	R3($k\Omega$)
-1	-1	-1	1	1	1	-1	8.46	5.17	8.37
-1	-1	1	1	-1	-1	1	1.28	1.40	1.79
-1	1	-1	-1	1	-1	1	1.79	2.50	3.77
-1	1	1	-1	-1	1	-1	1.14	1.11	1.20
1	-1	-1	-1	-1	1	1	3.05	3.00	3.54
1	-1	1	-1	1	-1	-1	0.97	0.86	1.00
1	1	-1	1	-1	-1	-1	1.46	1.14	1.25
1	1	1	1	1	1	1	0.94	0.26	0.17

Using linear regression analysis, the following linear model derived involves all the parameters for the main factors and their interactions.

$$R = \beta_0 + \beta_1 T + \beta_2 t + \beta_3 C + \beta_4 Tt + \beta_5 TC + \beta_6 tC + \beta_7 TtC \qquad \textbf{Eq 3-4}$$

where R is sheet resistance measured in kilo-ohm ($k\Omega$), T is temperature measured in centigrade (^{o}C), t is time measured in hours and C is concentration of the as-prepared ink measured in milligrams per millilitres (mg/ml). The values for the above linear regression model parameters listed in Table 3-4.

Table 3-4 linear regression parameters for **Eq 3-4**.

β_0	2.32
β_1	-0.85
β_2	-0.92
β_3	-1.30
β_4	-0.32
β_5	0.53
β_6	0.72
β_7	-0.36

According to the ANNOVA analysis, although the model is able to predict more than 95% (r-squared) of the variability of the data, its predictive behaviour is not desirable since it involves all the parameters in the full regression model. That is, it has 8 terms. To resolve this issue, natural logarithm of the sheet resistance was considered as the *y* value instead of sheet resistance. As a result, all the second order interactions were eliminated and the final model has only 4 terms including the third order interaction. Using linear regression analysis, the following linear model derived:

$$Ln(R) = \beta_0 + \beta_1 T + \beta_2 t + \beta_3 C + \beta_7 TtC \qquad \textbf{Eq 3-5}$$

The values for the above linear regression model parameters have been listed in Table 3-5.

Table 3-5 linear regression parameters for **Eq 3-5**.

β_0	0.33
β_1	-0.53
β_2	-0.26
β_3	-0.48
β_7	-0.24

Since parameters were derived based on the experimental values, the values need confidence intervals to be fully meaningful.

As a result of an orthogonal experimental design, we know:

$$Var(\beta_i) = 1/4\left(\frac{MSE}{R2^{K-2}}\right) \text{ and } SE = \sqrt{Var} \qquad \textbf{Eq 3-6}$$

where MSE is the estimate of the variance of the experimental error acting on the data, R is the number of independent replicates, K is the number of parameters and SE is standard deviation. Therefore, according to the values derived from ANOVA analysis:

$$Var(\beta_i) = 1/4\left(\frac{0.13615}{3 \times 2}\right) = 5.6729 \times 10^{-3} \xrightarrow{yields} SE = \sqrt{5.6729 \times 10^{-3}} = 0.075318$$

$$CI = \beta_i \mp t_{\frac{\alpha}{2},N-P}\, SE\,(\beta_i) \xrightarrow{yields} \beta_i \mp 2.1\,(0.075318) = \beta_i \mp 0.15816\,(i = 1,2,3,7)$$

$$Var(\beta_0) = Var\left(\frac{gt}{R2^K}\right) = \left(\frac{1}{R^2 2^{2K}}\right) Var(gt) = \left(\frac{1}{R^2 2^{2K}}\right) Var(y_1 + y_2 + \cdots) = \left(\frac{1}{R^2 2^{2K}}\right) n \times MSE$$

$$= \frac{24}{9} \times 2^6 \times 0.136 = 5.66 \times 10^{-3} \xrightarrow{yields} SE(\beta_0) = 0.07527$$

$$CI = \beta_0 \mp 0.158\,(i = 0)$$

Therefore, the confidence interval for all the linear regression parameters is the same.

Figure 3-8 represents all the values corresponding to the independent replicates and the model predictions for all the corners of the design space.

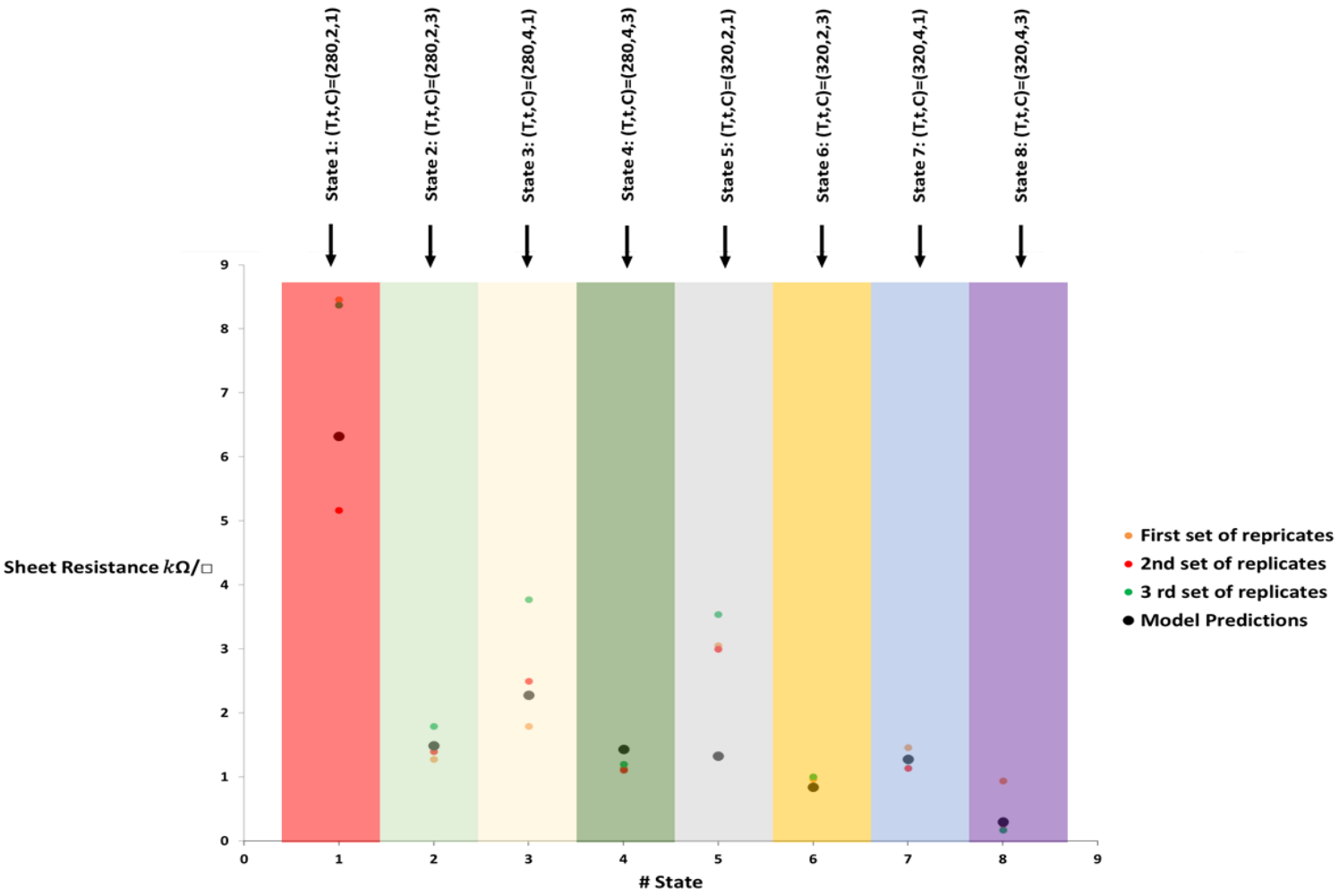

Figure 3-8 Representation of all the values corresponding to the independent replicates and the model predictions.

Figure 3-9 to Figure 3-11 illustrate the residual plots associated with the model (**Eq 3-5)**.

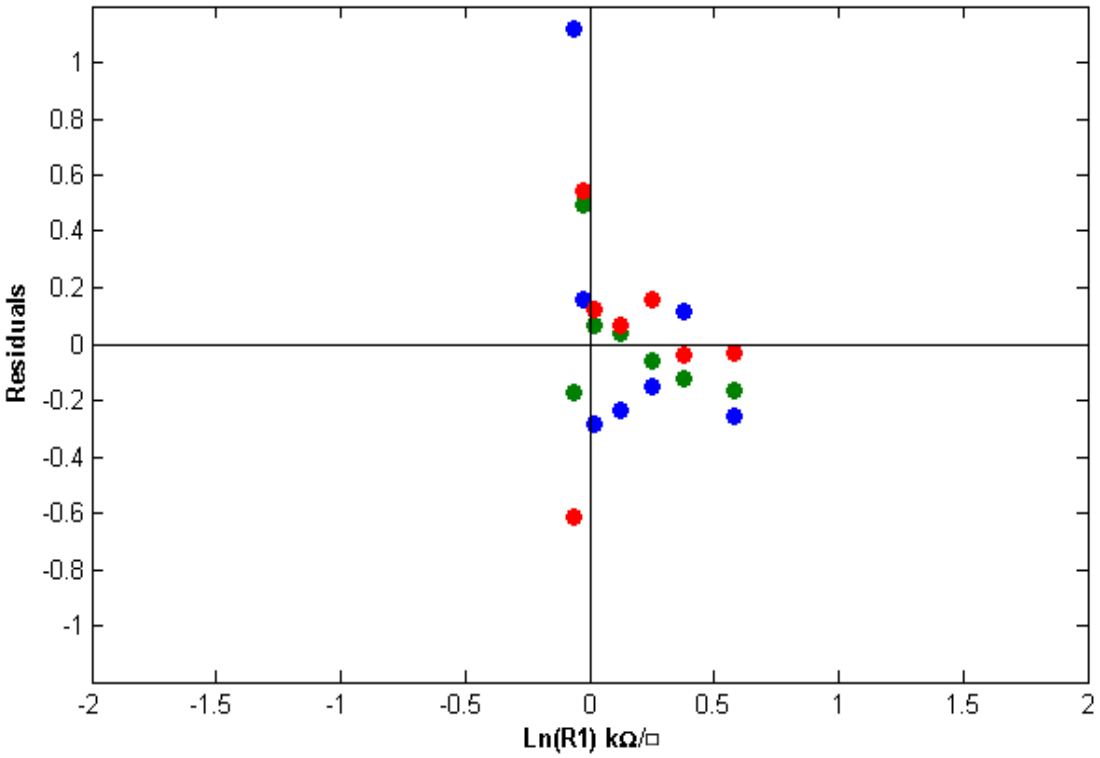

Figure 3-9 Residual plot vs the first set of replicates.

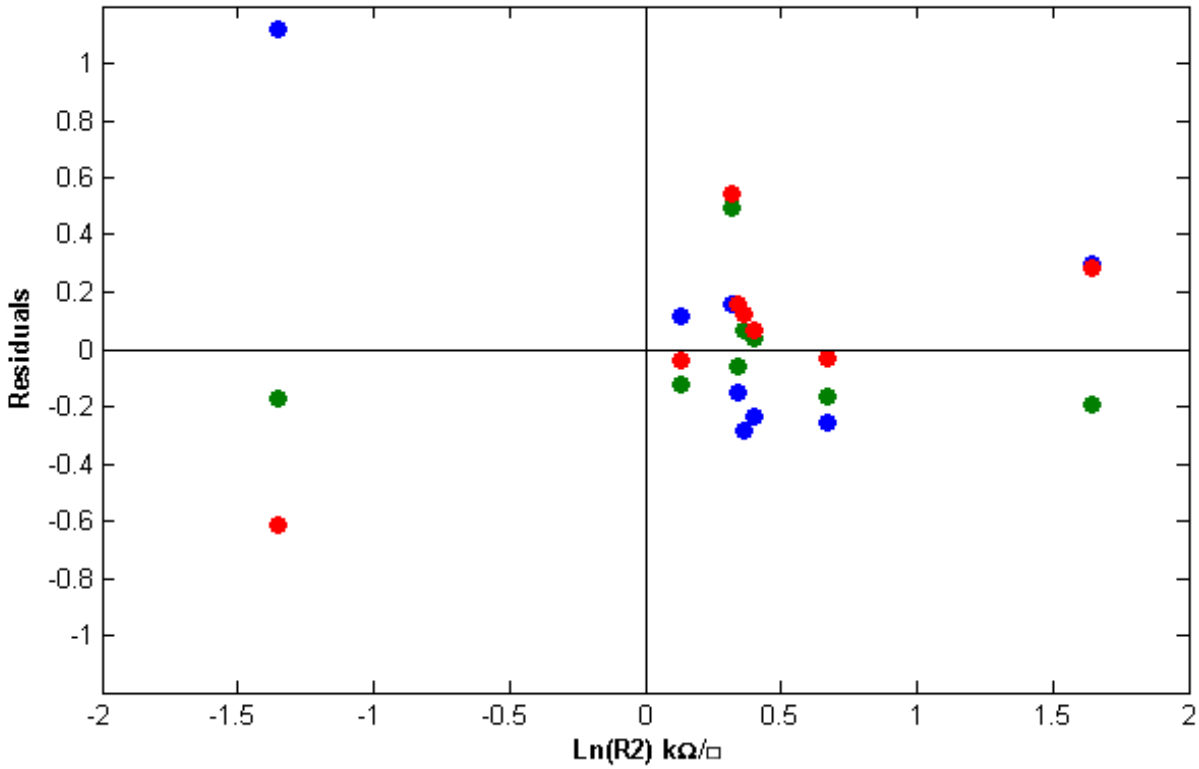

Figure 3-10 Residual plot vs the second set of replicates.

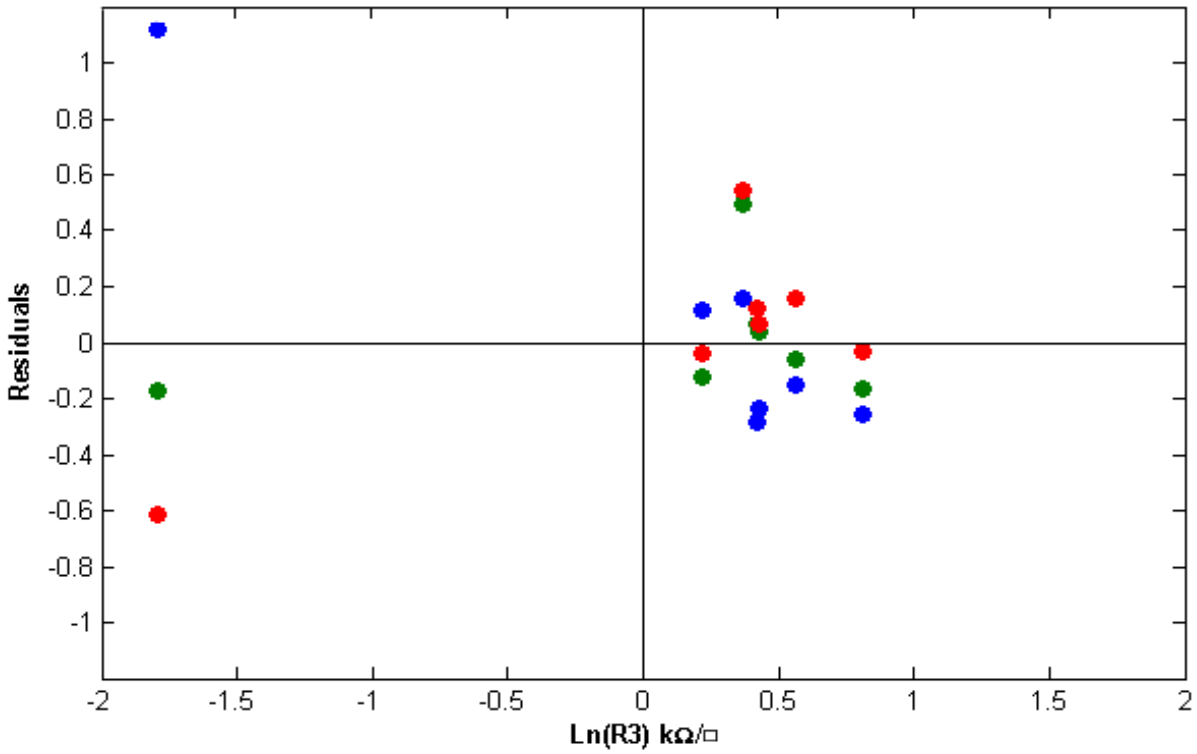

Figure 3-11 Residual plot vs the third set of replicates.

Although the gun-shot pattern of the residual plots confirms that the model is appropriate, center point replicates were made in order to ensure that the linear model does not have any curvature. That is, three independent replicates with 2 mg/ml ink concentration were fabricated and annealed at 300 ^{o}C for 3 hours. This corresponds to (0,0,0) in the orthogonal design space. Also, it is known that the best error estimate could be derived from center point replicates. Table 3-6 provides the information for these points.

Table 3-6 Center point replicates for sheet resistance modeling experiment.

	T (C°)	t (hrs)	C (mg/ml)	R ($k\Omega$)	model prediction
Sample #1	300	3	2	1.57	1.46
Sample #2	300	3	2	1.38	1.46
Sample #3	300	3	2	1.50	1.46

As demonstrated in Figure 3-12, the predicted values by the model are in a very good agreement with the measured values for the sheet resistance.

We have seen that our model is able to predict 88% (R^2) of the variability of the results.

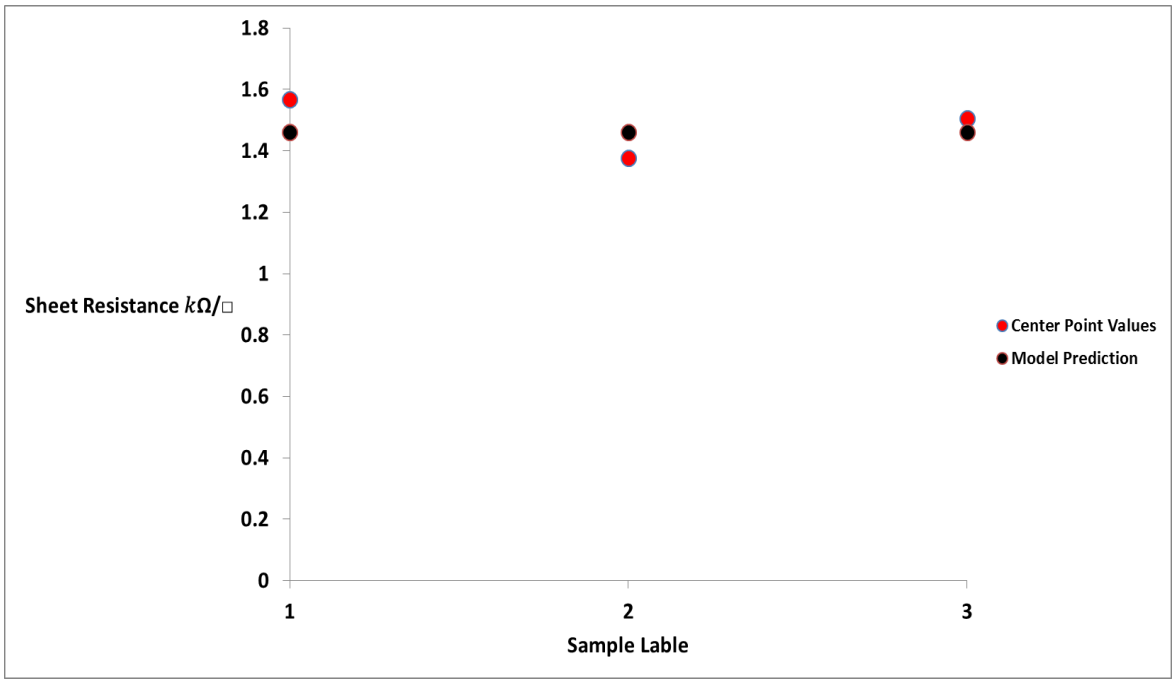

Figure 3-12 Center point replicates vs model prediction.

Figure 3-13 to Figure 3-15 illustrate the 3D plot of R at t =2 hours (corresponding to -1 in orthogonal design), t =4 hours (corresponding to +1 in orthogonal design) and t =3 hours (corresponding to 0 in orthogonal design). As demonstrated by the plots and the mathematical model, annealing temperature and the concentration of the as-prepared ink play the most important role in the sheet resistance of graphene paper, while annealing time and the third order interaction between the design variables are almost equally significant. Moreover, the values of confidence intervals for the parameters ensure the fact that the variance of the error acting on the experiment is small enough, and the predictability behaviour of the model should be acceptable enough for us to be able to interpolate other sheet resistances values inside the design window. Also, the mathematical model makes it possible to optimize the sheet resistance of graphene paper or get the desired sheet resistance based on the experimental condition that we have.

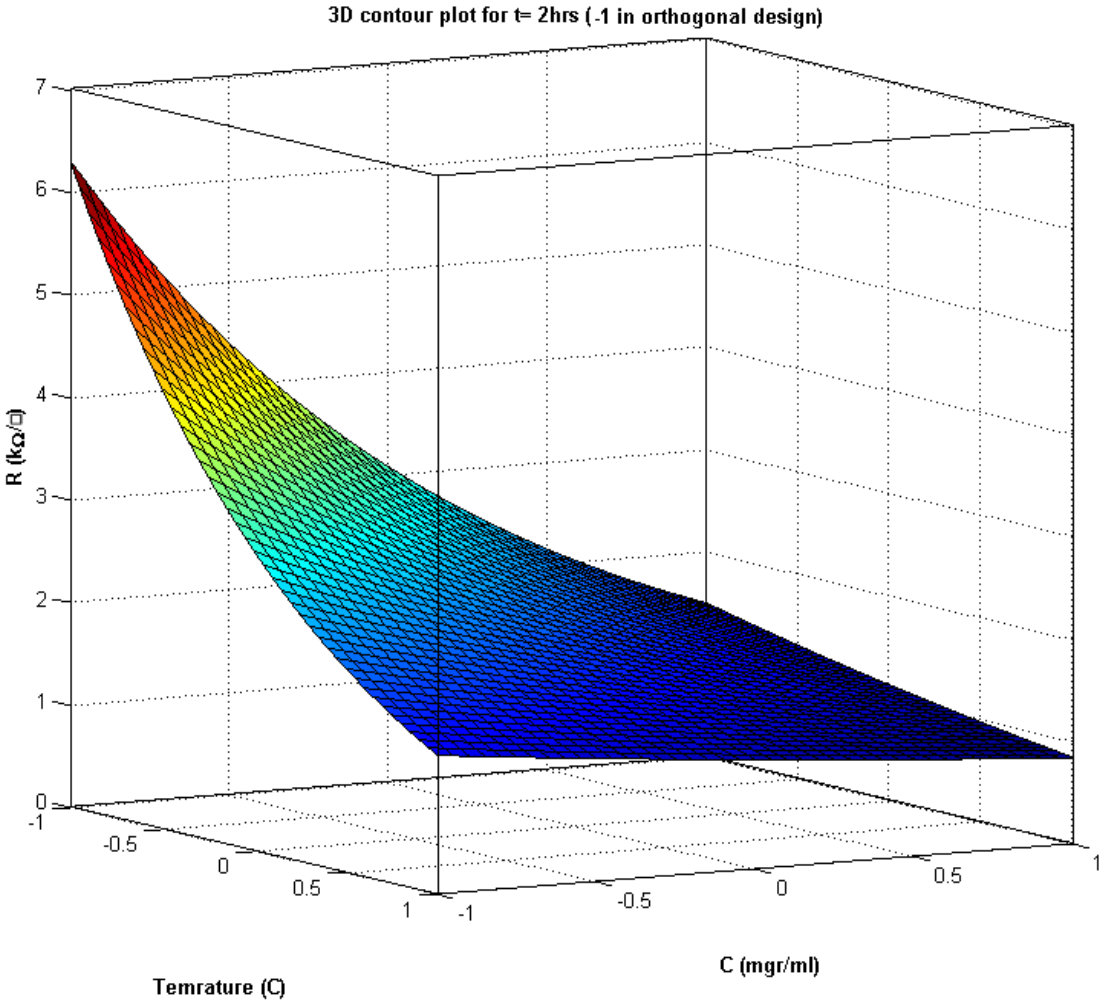

Figure 3-13 3D contour plot for t=2 hrs.

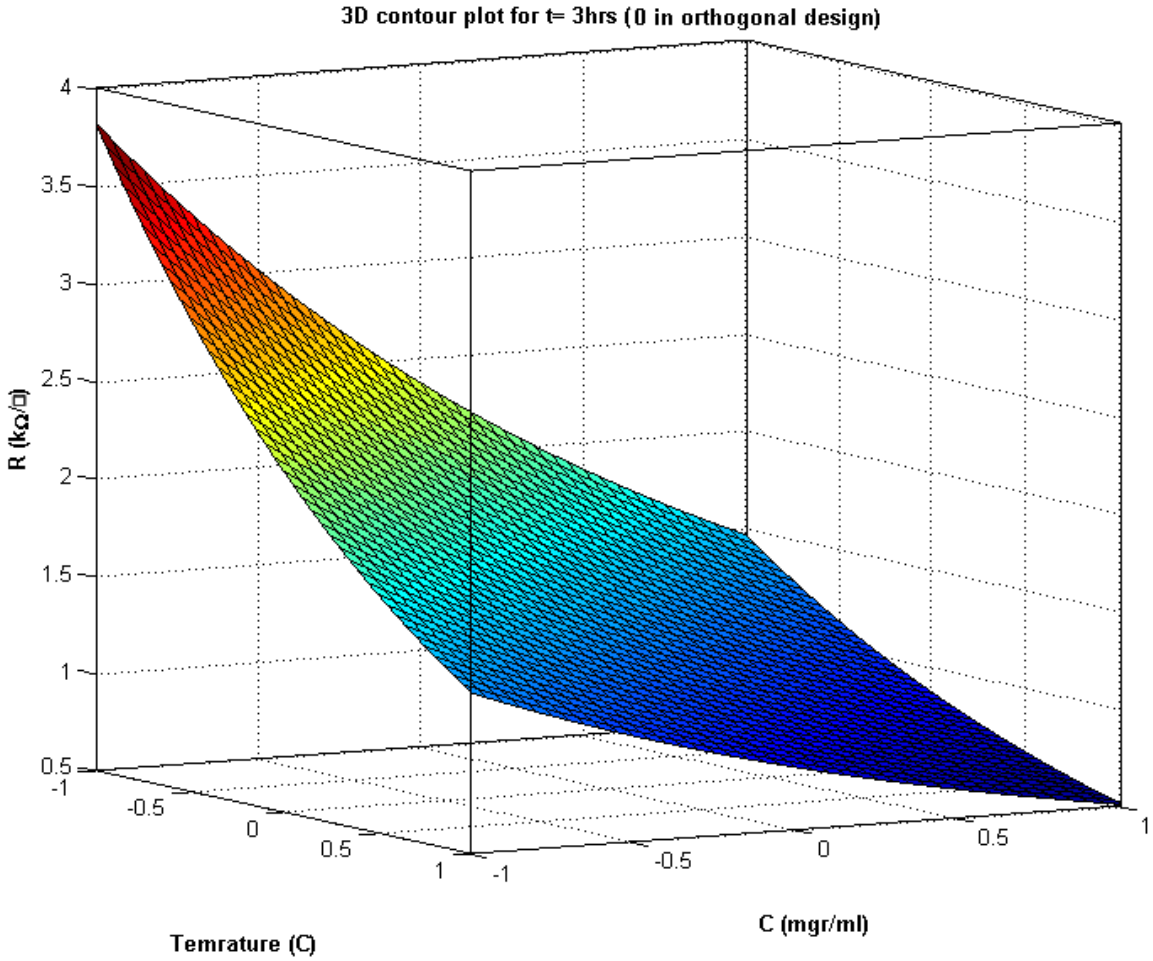

Figure 3-14 3D contour plot for t=3 hrs.

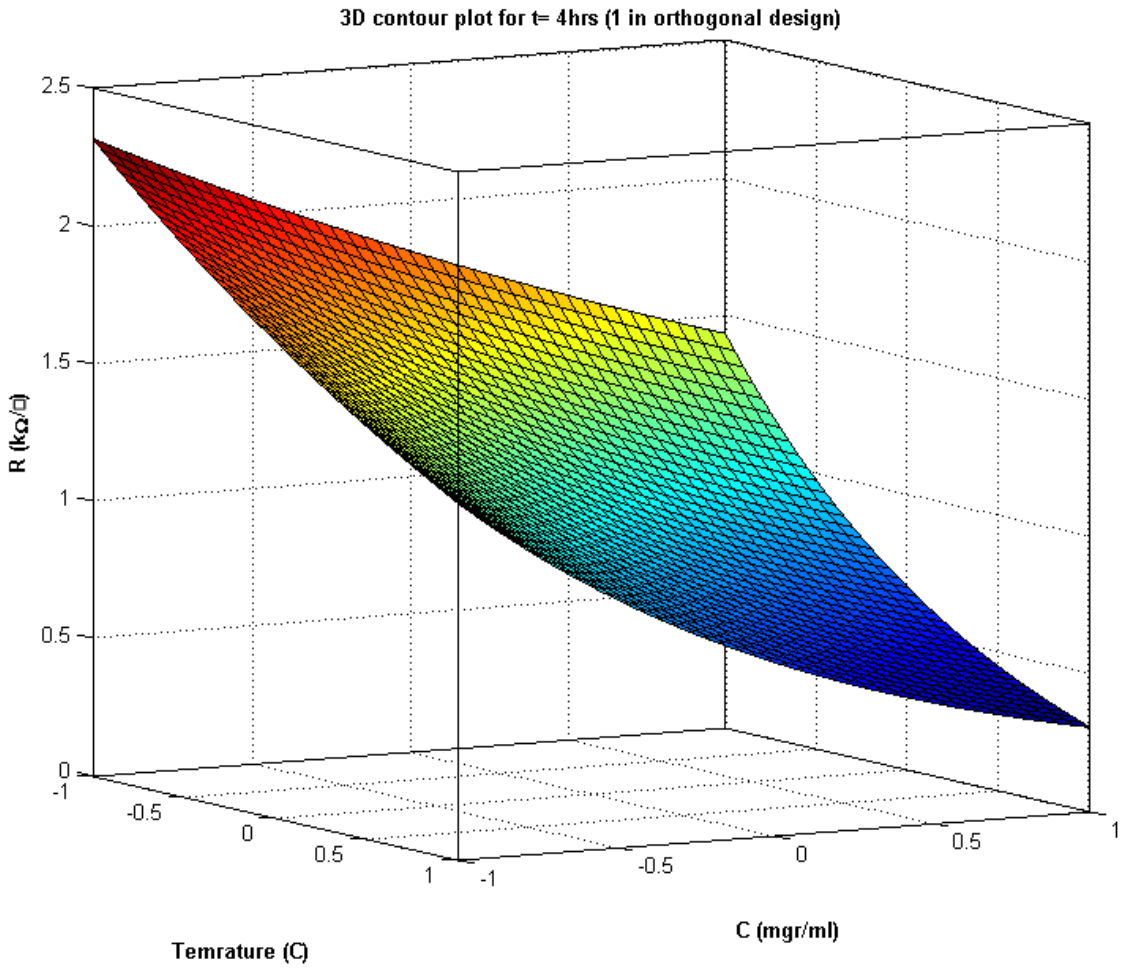

Figure 3-15 3D contour plot for t=4 hrs.

3.5 Cyclic bending Experiment

A bending fatigue test was conducted to study the effect of repeated bending on the electrical properties of graphene paper. The specimen used was the same size as in the sheet resistance tests. In this test, fifteen different samples with five different annealing times (Figure 3-5) were subjected up to 400 cycles to investigate the effect of cyclic bending on the graphene paper structures produced by different annealing times. In each cycle, to apply reproducible bending strains, each sample was completely bent over a cylinder with specific radius, held for a second and then released. The first 200 cycles were completed using an 8 mm radius of curvature, followed by 200 cycles using a 4 mm radius of curvature, as illustrated in Figure 3-16.

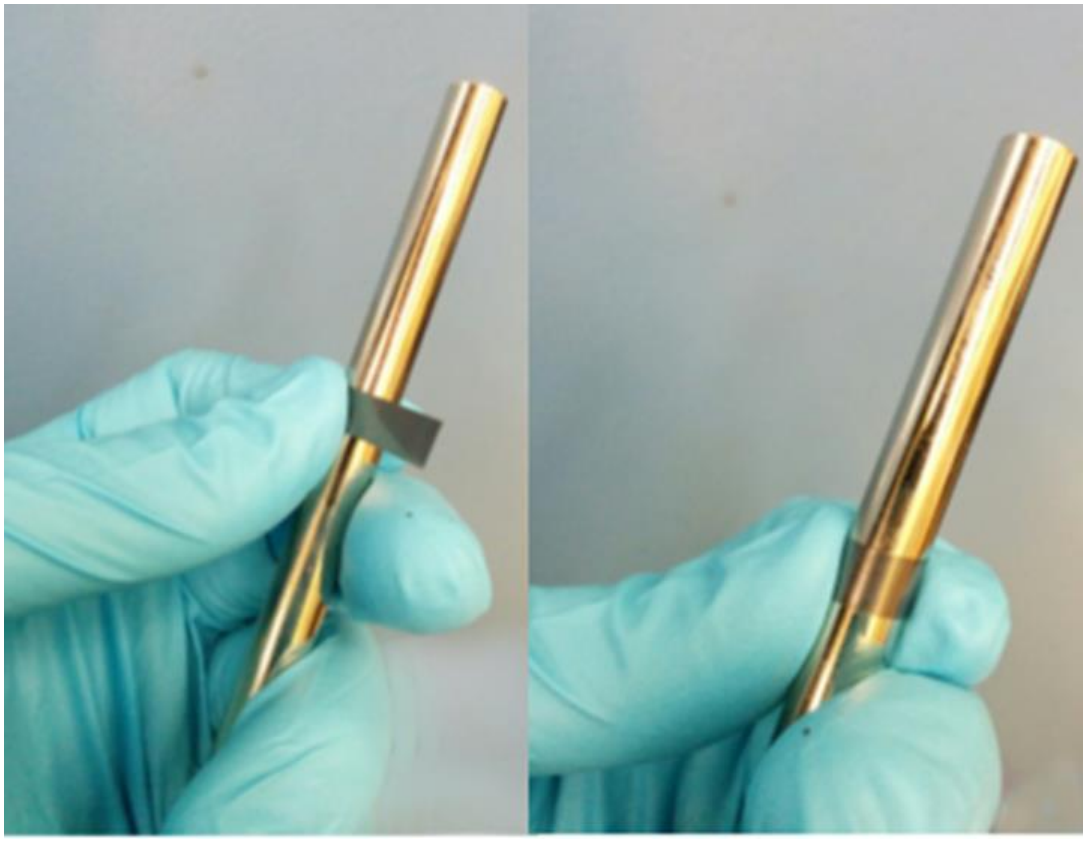

Figure 3-16 Fatigue bending graphene paper sample and set-up.

According to the plot in Figure 3-17, the resistance of the samples annealed for 40 minutes, 2 hours, 4 hours and 8 hours, respectively, does not change even after 400 bending cycles. However, the resistance of the sample annealed for 24 hours starts increasing moderately even after the first 50 cycles although the rate of its change did not increase when we decreased the radius of curvature.

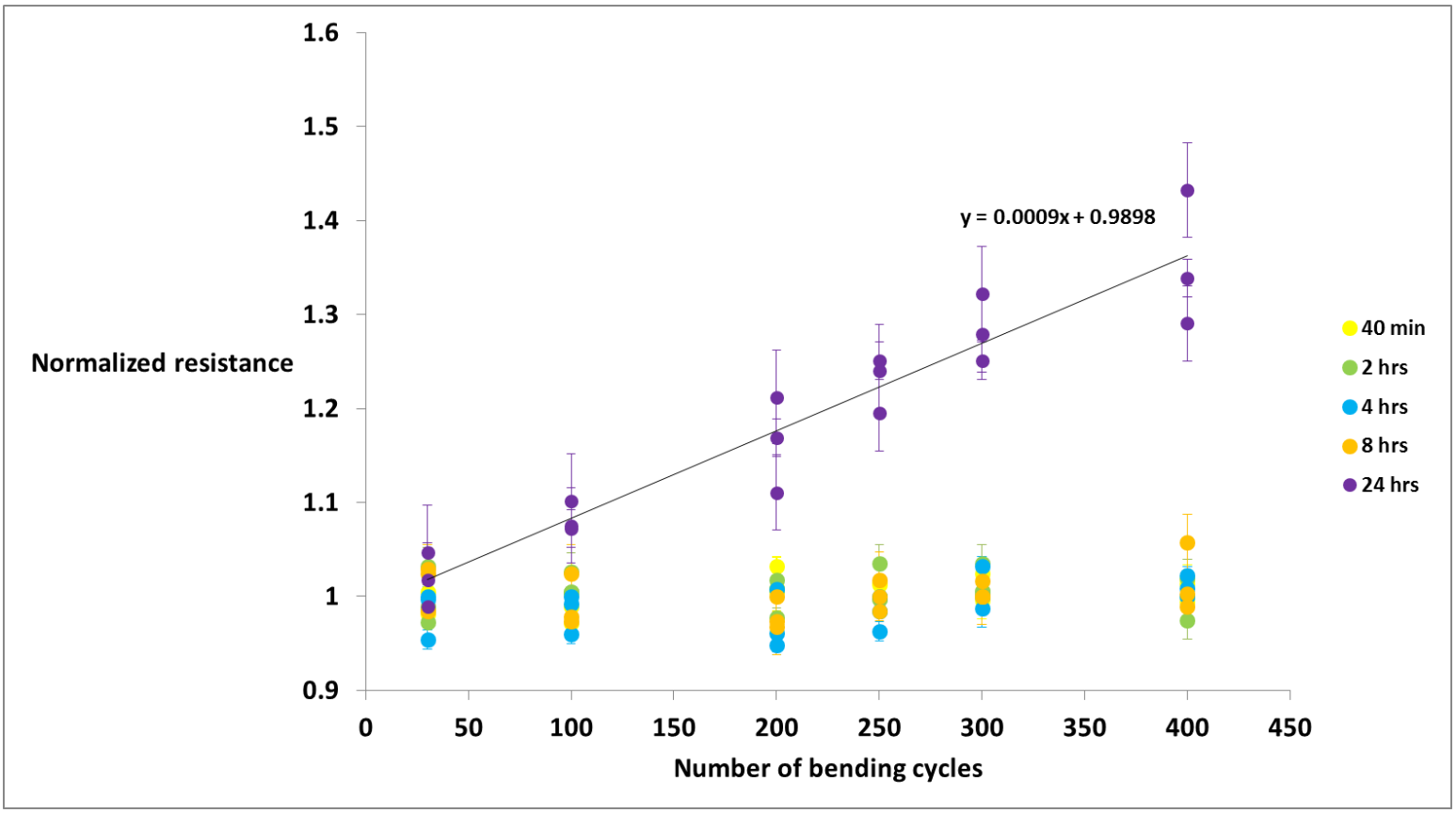

Figure 3-17 Normalized resistance vs number of bending cycles for cyclic bending experiment.

We have clearly demonstrated the existence of a trade-off between electrical and mechanical properties in our system [20]. In other words, although lower resistance can be achieved by increasing the annealing time, the structural properties of graphene paper are degraded. However, we could see that the resistance of all the samples except the one annealed for 24 hours almost remained the same after 400 bending cycles. This suggests that the lowest resistance measured here can be maintained over the course of 400 bending cycles. These results are also consistent with the excellent mechanical and electrical properties of the structures made out of graphene blocks [38, 42].

3.6 Adhesion Tests

Figure 3-18 illustrates the free body diagram of the sample mounted on the adhesion test setup described in Chapter 2. Accordingly, the force acting on the surface of the graphene paper should be known.

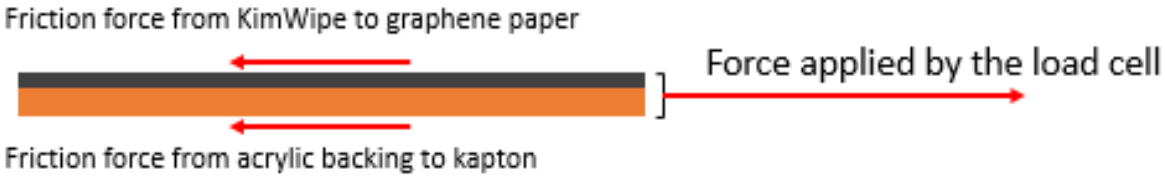

Figure 3-18 Free body diagram of graphene paper coating with Kapton substrate mounted on the adhesion test setup.

It is noted that the force from load cell is applied to the graphene paper and kapton substrate at the same time since they are held by the film gripper attached to the end of the load cell. Also, Figure 3-18 represents an equation with two unknowns since the coefficient of the kinetic friction between acrylic and kapton is not known. For this, an estimate is required before conducting the adhesion experiment. To do so, a kapton film without any graphene coating was mounted on the setup. An acrylic block with a known mass was placed on the kapton. The coefficient of kinetic friction between kapton and acrylic could be derived since the same material has been used above and underneath the sample. As a result, this value was calculated to be $\mu_{k\ (Acrylic-Kapton)} = 0.2$

Newton's first law applies for the adhesion test because the sample is pulled with constant velocity. Therefore:

$$\sum F = 0 \longrightarrow F_{Loadcell} - F_{Acrylic-Kapton} - F_{KimWipe-Graphene} = 0 \longrightarrow \quad \textbf{Eq 3-7}$$

$$F_{KimWipe-Graphene} = F_{Loadcell} + F_{Acrylic-Kapton} = F_{Loadcell} + \mu_{k\ (Acrylic-Kapton)}\, mg$$

where m is the mass of the weights put on the top of the KimWipe measured in kg and g is gravitational acceleration measured in m/s^2.

Figure 3-19 to Figure 3-23 illustrate the normalized resistance of samples with different annealing temperature based on the amount of shear force applied on the surface of graphene paper.

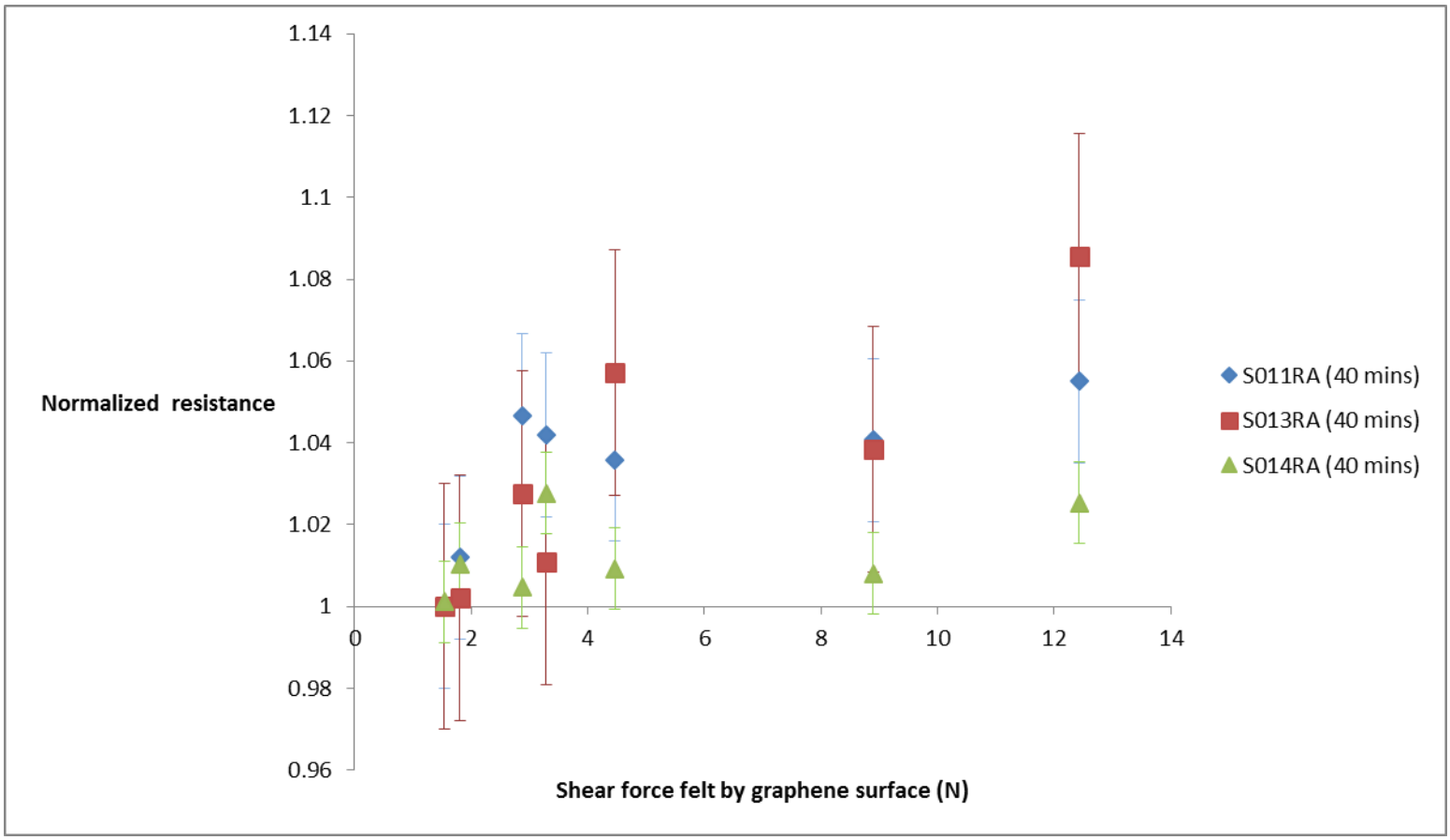

Figure 3-19 Normalized resistance vs shear force for 40 mins annealed samples.

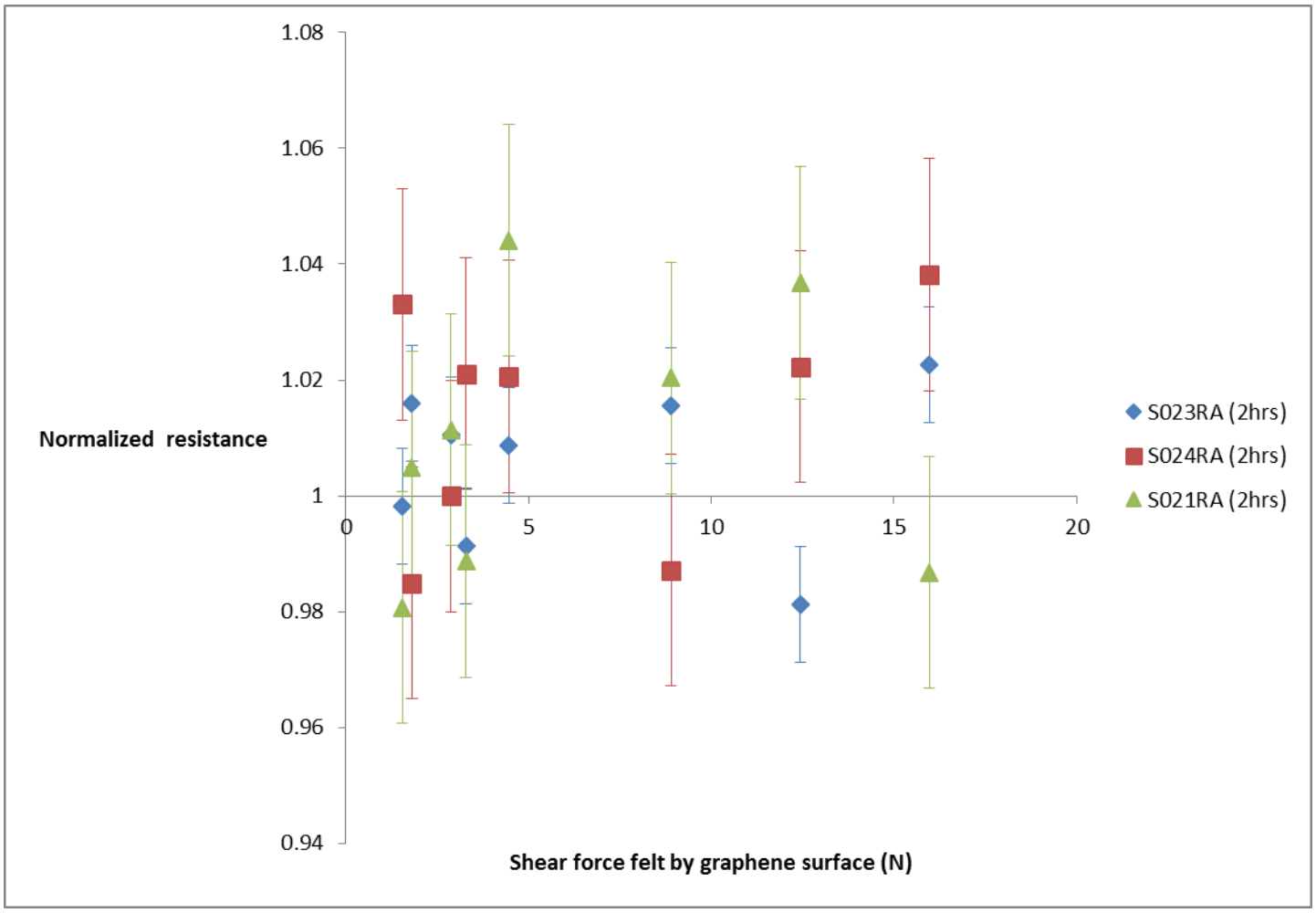

Figure 3-20 Normalized resistance vs shear force for 2 hrs annealed samples.

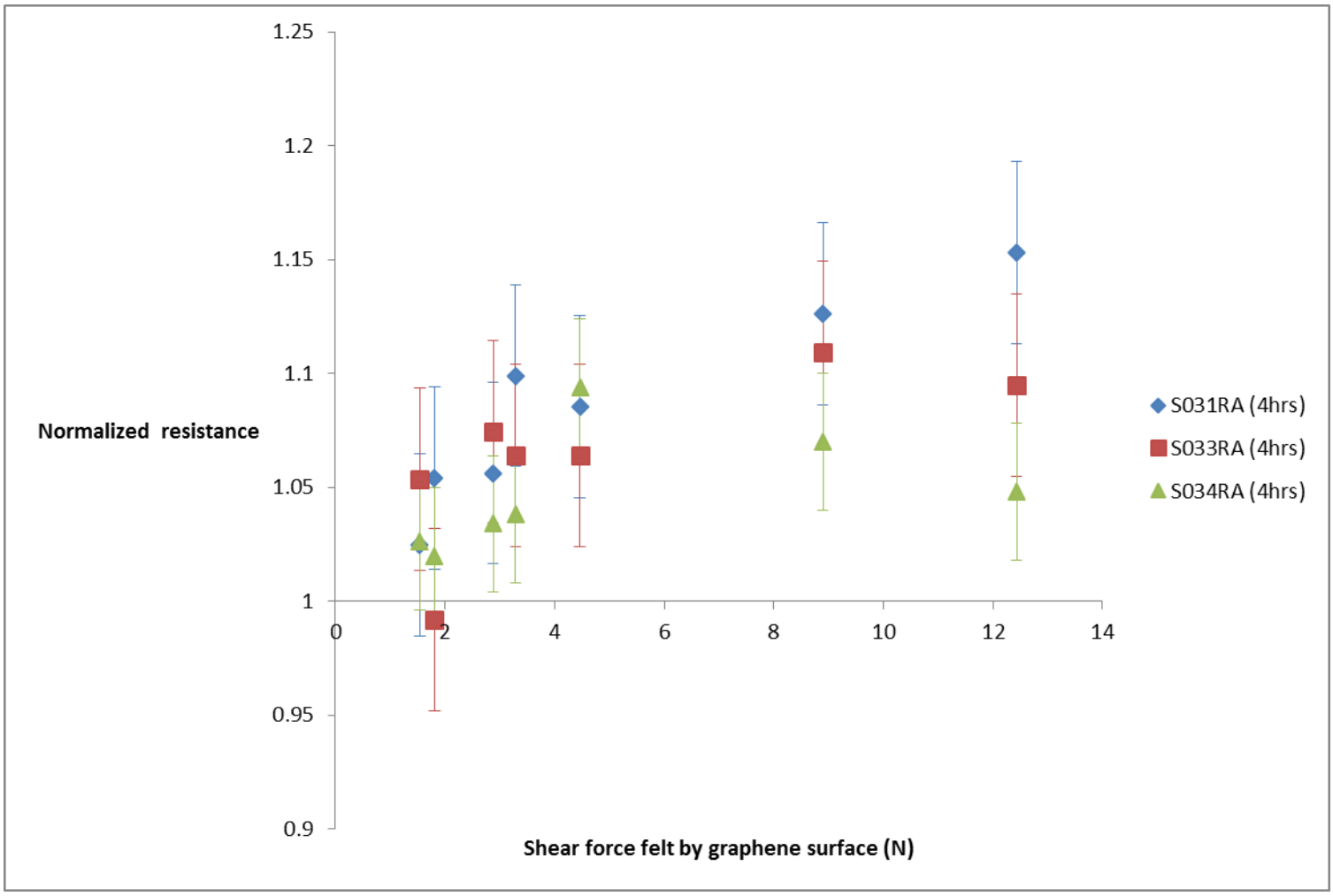

Figure 3-21 Normalized resistance vs shear force for 4 hrs annealed samples.

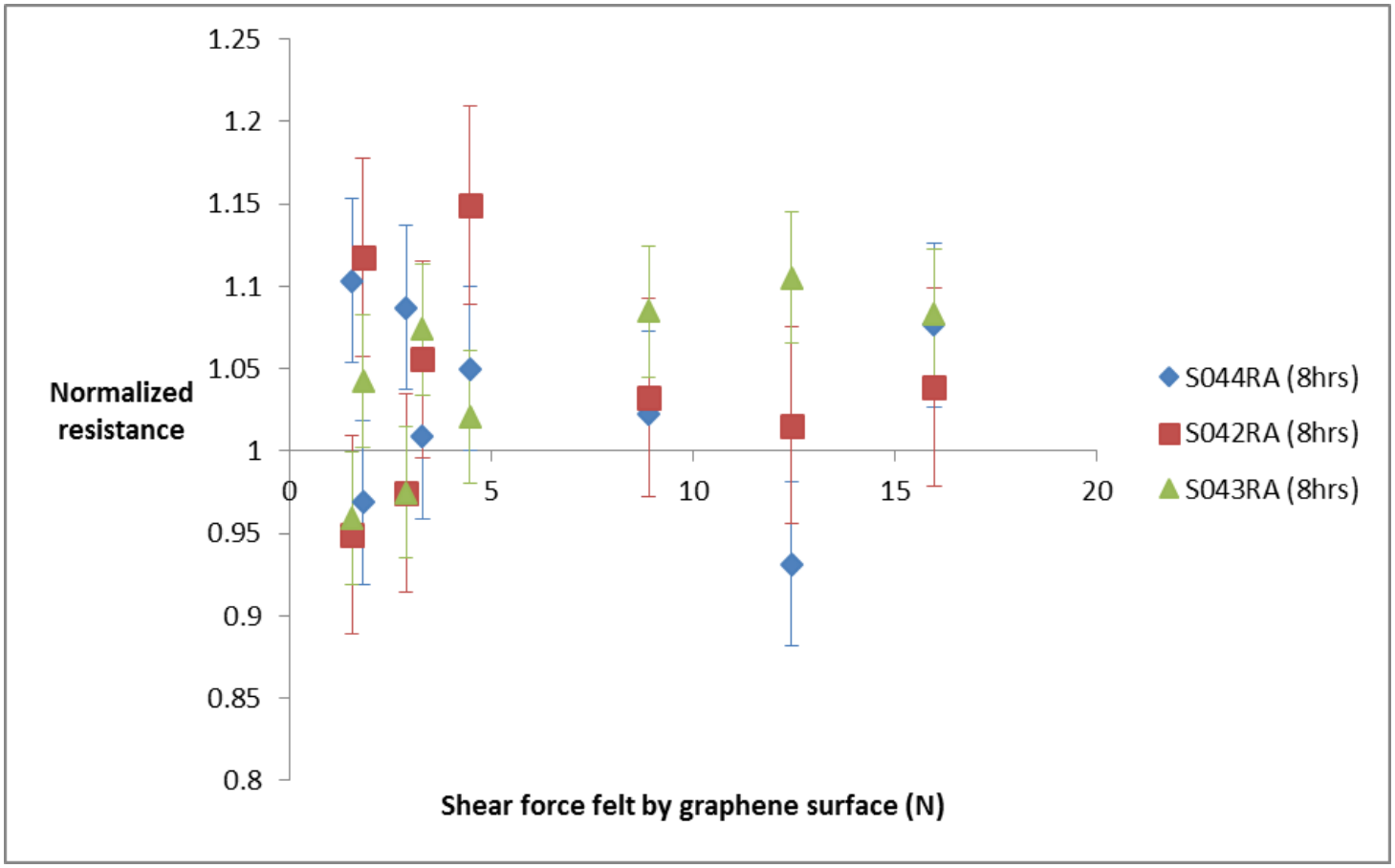

Figure 3-22 Normalized resistance vs shear force for 8 hrs annealed samples.

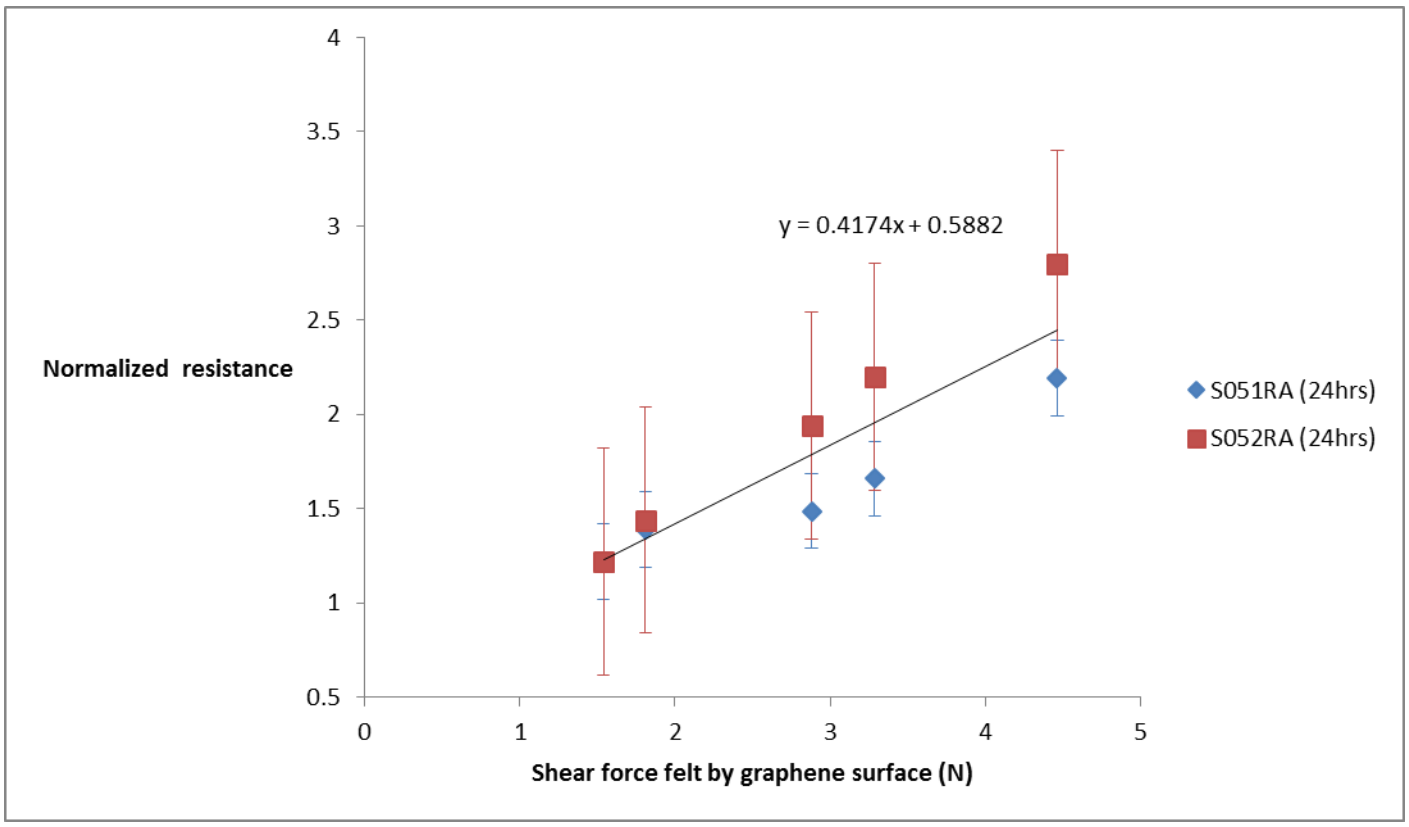

Figure 3-23 Normalized resistance vs shear force for 24 hrs annealed samples.

Examinig Figure 3-19 to Figure 3-23, the mechanical properties of graphene paper deteriorates as the annealing time increases. Whether or not the change is significant depends on the particular service application. However, it is clear that the rate at which the resistance changes are considerably higher for 24 hour-annealed sample than the others.. These results are also consistent with the fatigue bending tests. Moreover, cohesive failure was not observed for samples annealed at 40 min and 2 hours at all although this was observed for samples annealed at 4 hours and 8 hours at 10 N. Samples annealed for 24 hours showed a very brittle structure with the first signs of cohesive failure at force values lower than 5 N.

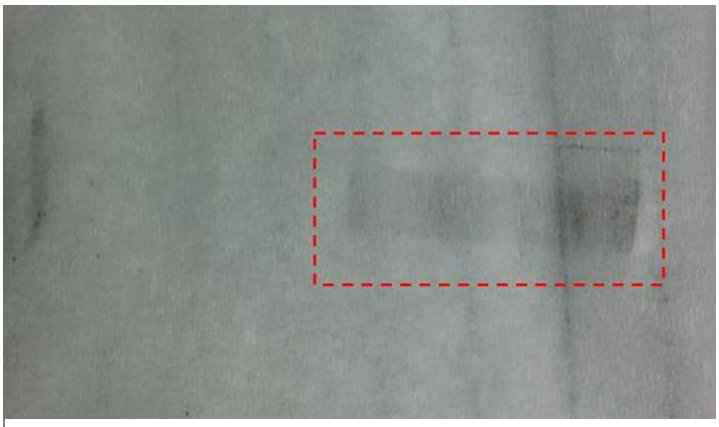

Figure 3-24 Cohesive failure of graphene paper on soft tissue, KimWipe.

3.7 Elastic Modulus and Tensile Strength Measurements

There is a limited number of work where free-standing or monolithic graphene paper has been tested in tension to determine elastic modulus and tensile strength propertes [20, 60]. In the knowledge of the author, no evaluation of graphene paper coatings prepared by our process exists in the open litrature. We conducted a simple experiment to determine if it is possible to reliably measure these mechanical properties. A set of iso-strain experiments for three different uncoated kapton samples at three levels of strain. Two duplicate measurements at each test were conducted using a dynamic mechanical analyzer (DMA, TA instruments Model Q800). A thin film tension clamp was used. Table 3-7 summarizes the measured force results for the three uncoated samples:

Table 3-7 Force measurements for uncoated Kapton samples.

Strain %	Force (N)		
	Sample #1	Sample #2	Sample #3
0.1	2.691	2.587	2.603
	2.532	2.607	2.508
0.15	3.758	3.8	3.908
	3.839	3.299	3.953
0.2	5.297	5.298	5.243
	5.372	4.993	5.15

Since duplicate measurements are not independent replicates, it is best to use their averages in the statistical calculations. Therefore, Table 3-8 was used for the analysis.

Table 3-8 Force values used for statistical analysis.

Strain %	Force (N)			
	Sample #1	Sample #2	Sample #3	Row Sum
0.1	2.6115	2.597	2.5555	7.764
0.15	3.7985	3.5495	3.9305	11.2785
0.2	5.3345	5.1455	5.1965	15.6765
Column Sum	11.7445	11.292	11.6825	

S_C is the correction for the mean. The sum of all the observations squared over the total number of observations.

$$S_C(correction\ for\ the\ mean) = \frac{1}{3 \times 3}\ (gt)^2 = \frac{1}{9}\ (34.719)^2 = 133.934 \quad \textbf{Eq 3-8}$$

S_D, which is the difference between sum of squared observations and correction for the mean, is used to calculate the variability of the desired factors.

$$S_D = Sum\ of\ squared\ observations - S_C = 144.508 - 133.934 = 10.574 \quad \textbf{Eq 3-9}$$

Calculating the variability of the samples:

$$S_{Sample} = \left(\frac{1}{n}\right) \times Sum\ of\ squared\ Coloumn\ Sum\ - S_C \quad \textbf{Eq 3-10}$$

$$= \left(\frac{1}{3}\right) \times (11.7445^2 + 11.292^2 + 11.6825^2) - 133.934 = 0.04$$

Calculating the variability of the strain levels:

$$S_{Strain} = \left(\frac{1}{n}\right) \times Sum\ of\ squared\ Row\ Sum - S_C \quad \textbf{Eq 3-11}$$

$$= \left(\frac{1}{3}\right) \times (7.764^2 + 11.2785^2 + 15.6765^2) - 133.934 = 10.4$$

Calculating the variability of the error acting on the experimental data:

$$S_E = S_D - \left(S_{Sample} + S_{Strain}\right) = 10.574 - 10.4 - 0.04 = 0.134 \quad \textbf{Eq 3-12}$$

Now, the ANOVA table could be constructed:

Table 3-9 ANOVA table.

	SS	df	MS	F_{obs}
Sample	0.04	2	0.02	0.746269
Strain	10.4	2	5.2	194.0299
Error	0.134	5	0.0268	
Total	10.574	9		

Also, $F_{Critical}(2,5,0.05) = 5.7$ (considering the probability level of 5%)

Therefore, it can be concluded that the three samples used in this experiment are practically the same. This was predictable since the samples were cut from the same kapton sheet - all the samples can be assumed to have the same mechanical properties. Based on the ANOVA table, the variance of the error acting on this experiment is approximately 0.03.

It is also reasonable to assume that the variance of the errors acting on both experiments is almost the same since the handling procedure, methods and instruments used in both coated and uncoated Kapton experiments are the same.

As a result, the difference between the means of graphene paper coated Kapton films and uncoated Kapton films should be statistically significant in order for the graphene paper to have a significant effect in the force measurements. Therefore:

$$\frac{\bar{F}_{Coated\ films} - \bar{F}_{Uncoated\ films}}{S_p\sqrt{\frac{1}{n_1}+\frac{1}{n_2}}} > t_{\left(\frac{\alpha}{2},\nu\right)} \quad \textbf{Eq 3-13}$$

$\upsilon = n_1 + n_2 - 2$ and ${S_p}^2 = \frac{(n_1-1){S_{p1}}^2+(n_2-1){S_{p2}}^2}{(n_1-1)+(n_2-1)}$

Substituting the values for 0.1% strain:

$$\frac{\bar{F}_{Coated\ films} - 2.6}{0.03\sqrt{\frac{1}{3}+\frac{1}{3}}} > t_{(0.025,4)} \longrightarrow \frac{\bar{F}_{Coated\ films} - 2.6}{0.03\sqrt{\frac{1}{3}+\frac{1}{3}}} > 2.13 \longrightarrow \bar{F}_{Coated\ films} > 2.65 \longrightarrow$$

$$Min(\bar{F}_{Coated\ films}) \cong 2.7$$

Also, for a film under tensile stress we have:

$$F_1 = \frac{AE}{l}\,\delta \xrightarrow{K_1=\frac{AE}{l}} F_1 = K_1\,\delta \qquad \textbf{Eq 3-14}$$

where A is the cross section of kapton film.

When coated with graphene paper:

$$F = \frac{E}{l}\,(A + td)\,\delta$$

where t is the thickness of the graphene paper, and d is the width of the sample. Therefore:

$$K_2(kapton\ films\ coated\ with\ graphene\ paper) = K_1 + \frac{td\ E_{graphene\ paper}}{l}$$

Based on the values measured by DMA for 0.1% strain:

$$K_1 = \frac{AE}{l} = (10 * 0.07) * \frac{3500}{20} = 122.5\frac{N}{mm}$$

$$F_2 = K_2\delta = \left(122.5 + \frac{td\ E_{graphene\ paper}}{l}\right) \times 0.1\ \times 10^{-2} \times 20 = 2.7 \longrightarrow$$

$$\left(122.5 + \frac{(t\ E_{graphene\ paper})10}{20}\right) \times 0.1\ \times 10^{-2} \times 20 = 2.7 \longrightarrow$$

$$Min\left(t\ E_{graphene\ paper}\right) = 25 \qquad \textbf{Eq 3-15}$$

Eq 3-15 specifies the theoretical minimum requirements for the thickness and the elastic modulus of graphene paper to have statistically significant mechanical effect in comparison with uncoated kapton films. The behaviour is illustrated in Figure 3-25. It could be understood that the effect of mechanically weak graphene paper could be captured if the coating is thick enough. However, in practical terms, even if 1 μm thick coating is achieved, it may not be possible to obtain an elastic modulus of ~ 50 GPa. Although Figure 3-25 suggests that a 50 GPa modulus can be obtained, the value

is considerably higher than the strongest graphene papers ever reported [20]. Moreover, it is widely known that the mechanical properties of graphene paper dramatically deteriorate as the thickness of the structure increases due to the weak intralayer cross links and high concentration of lattice defects. Furthermore, the maximum thickness achieved in this study is about 200-300 nm according to AFM analysis. This requires a graphene paper with elastic modulus as high as 100 GPa which is not practically achievable [20-23]. In addition, several preliminary experiments have been done by DMA which confirmed that the effect of the coating could not be captured. In the similar way, the same calculations and reasoning apply on ultimate tensile strength. Also, as mentioned in Chapter 1, graphene has been gaining more interests among researchers primarily because of its electronic properties and flexibility although it has proven to have superior mechanical properties when used in the form of a monolayer.

As a result, it has to be concluded that it is not feasible to measure the elastic modulus and ultimate tensile strength of graphene paper coating even by using highly precise measuring techniques such as the DMA.

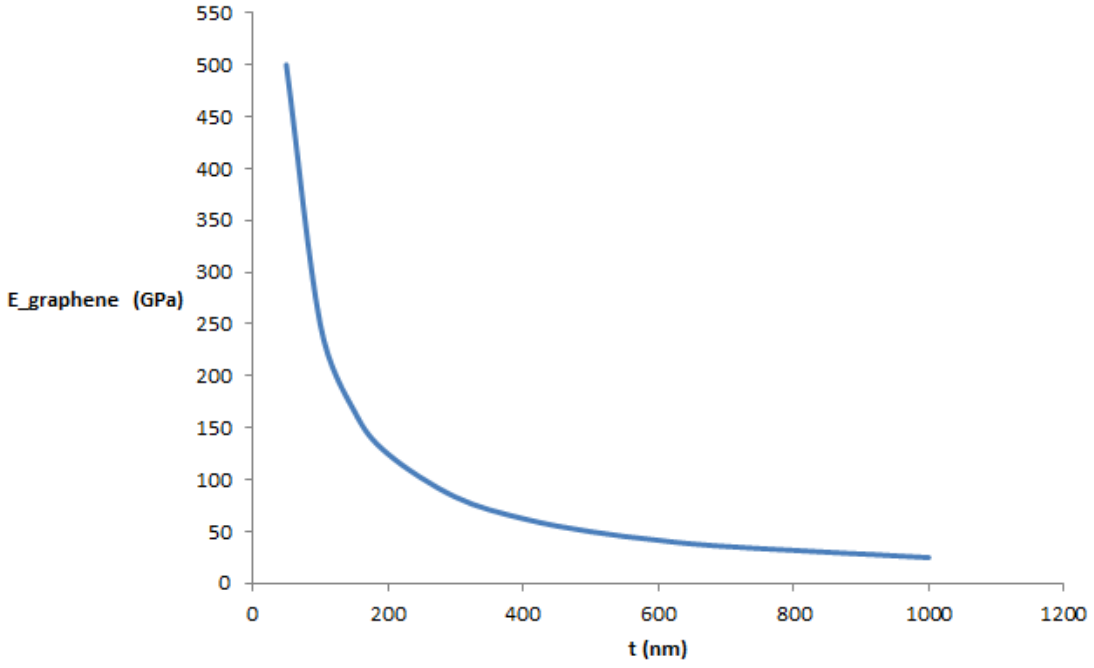

Figure 3-25 Elastic modulus vs thickness of graphene paper as per **Eq 3-15**.

3.8 Raman spectroscopy

A Bruker SENTERRA II Compact Raman Microscope with a 532 nm source laser set to 20 mW was used to scan the samples to both confirm phase purity and to understand the effect of annealing time on the concentration of graphene nano platelets in the graphene paper structure.

Raman spectroscopy results were taken from three different samples with three different annealing times. Previously, it was speculated that as annealing times increase, EC decomposition will increase and the nano platelets will have increased opportunity to align with each other. This is consistent with the narrower and sharper peaks of the sample annealed for 24 hours, as shown in Figure 3-26. Since the intensity of the peaks varies depending on the time over which the sample is being scanned, all the peaks are normalized based on the intensity of the maximum peak for that particular sample. The well-known G band appears around 1587 cm^{-1} and it is the in-plane vibrational mode which involves the sp^2 hybridized carbon atoms that comprises the graphene sheet [63]. The D band appears around 1350 cm^{-1} and is typically weak in highly pure Graphene since it's a measure of lattice disorder. The ratio of ID/IG has been broadly used to characterize the lattice structure of the graphene products. Lower ratios indicate fewer defects and less lattice disorder in the structure. Table 3-10 provides information about ID/IG for all the samples. The low ratio of ID/IG demonstrates high quality graphene paper as the building structure of the paper. However, due to the nature of paper materials which are hierarchical structures made out of millions of small units, the presence of edge defects is inevitable, creating a D band in the Raman spectrum. Also, the 2D band which is the second order of zone boundary phonons appears around 2700 cm^{-1}. This band is always strong in the graphene structures since it does not need to be near the defects to be activated [63, 64].

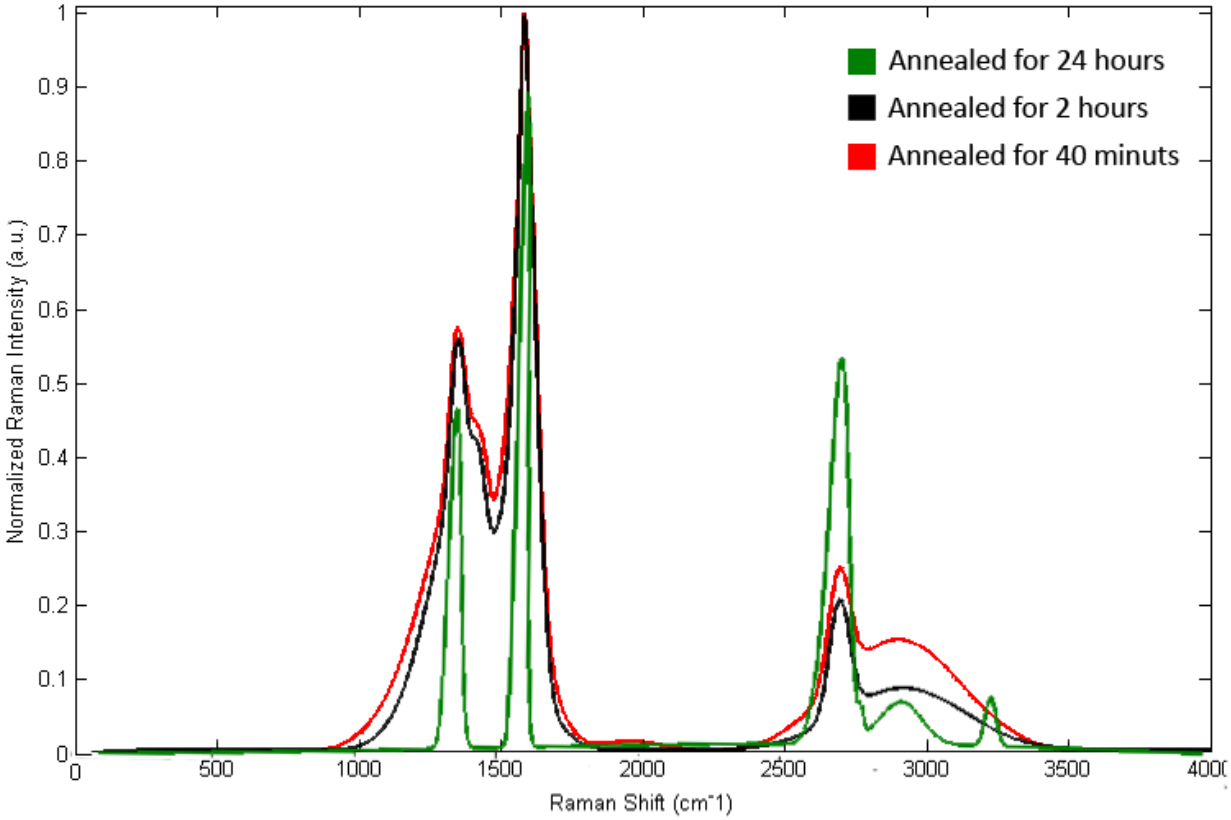

Figure 3-26 Raman spectroscopy results for three different samples.

Table 3-10 ID/IG ratio for Raman spectroscopy results.

Sample #	ID/IG
S1 (40 min)	0.6
S2 (2 hrs)	0.57
S3 (24 hrs)	0.49

3.9 Super Capacitance Measurements

First, the electrodes have been heated at 300 ^{o}C for an hour. Longer annealing times have been attempted before which caused undesirable Ni oxidization. The electrodes have been tested in a cyclic voltammetry test device. However, no significant capacitance behaviour was observed. This could be attributed to the high electrical resistance of the active material at this temperature for this specific cyclic voltammetry test. The capacitance of the electrodes, however, was found to improve by increasing the annealing temperature up to 500 ^{o}C. Further temperature increase not only caused Ni oxidization even in relatively short annealing times, but also led to minimal change in capacitance behaviour. Oxidization of the Ni as the current collector has detrimental effects on the electrode system since it increases both the resistance of the current collector, itself, and the contact resistance between current collector and the active material. Figure 3-27 illustrates the CV curves for Ni-Graphene electrode and 2 molar KOH as aqueous electrolyte.

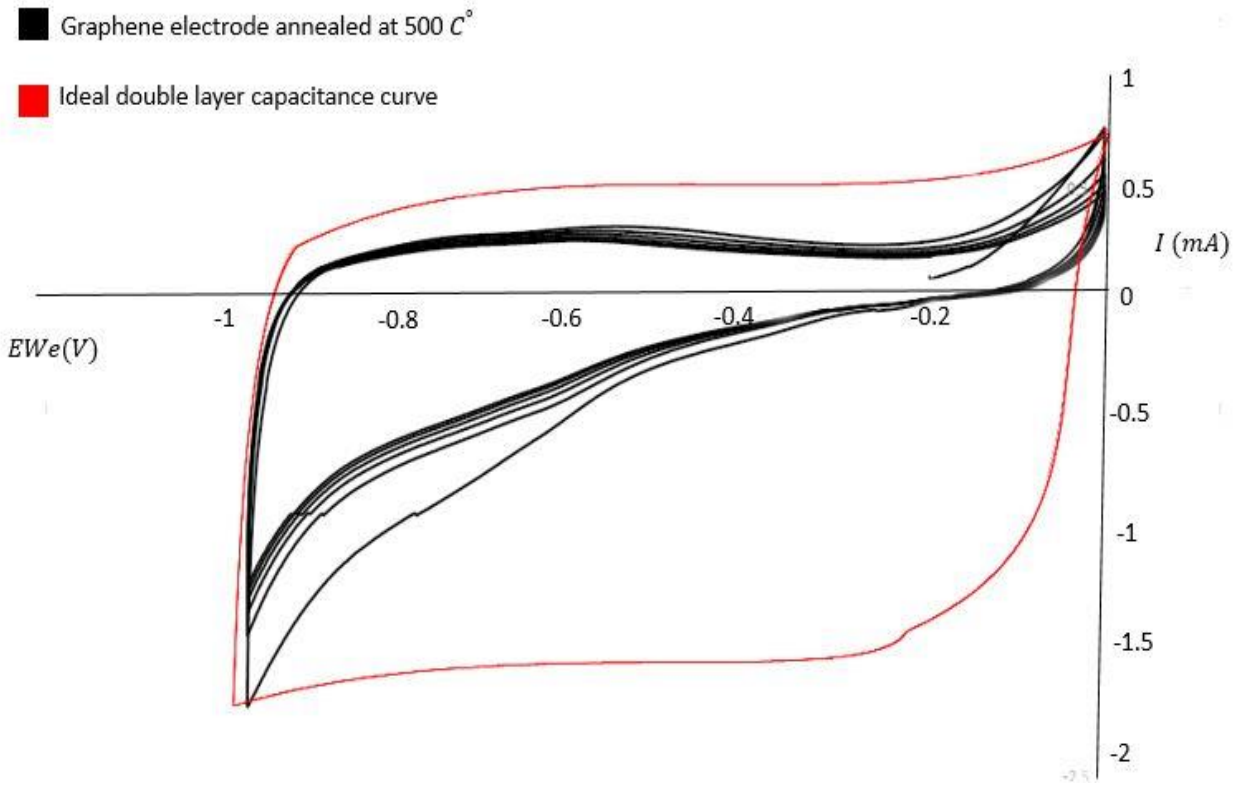

Figure 3-27 CV curves for Graphene/Ni electrode and ideal double layer behavior.

The red plot in Figure 3-27demonstrates an ideal double layer capacitance behaviour. It can be seen that even if the material exhibits an acceptable capacitance behaviour in charge cycles, it demonstrates a large fall off in discharge cycles. This could be attributed to the small pores and low surface area of the graphene coating [41]. This was confirmd by SEM images taken from the surface of the graphene paper as shown in Figure 3-28. SEM images were obtained using JEOL JSM-7000F machine and at 2.0 kV voltage with 5000 and 20000 magnification.

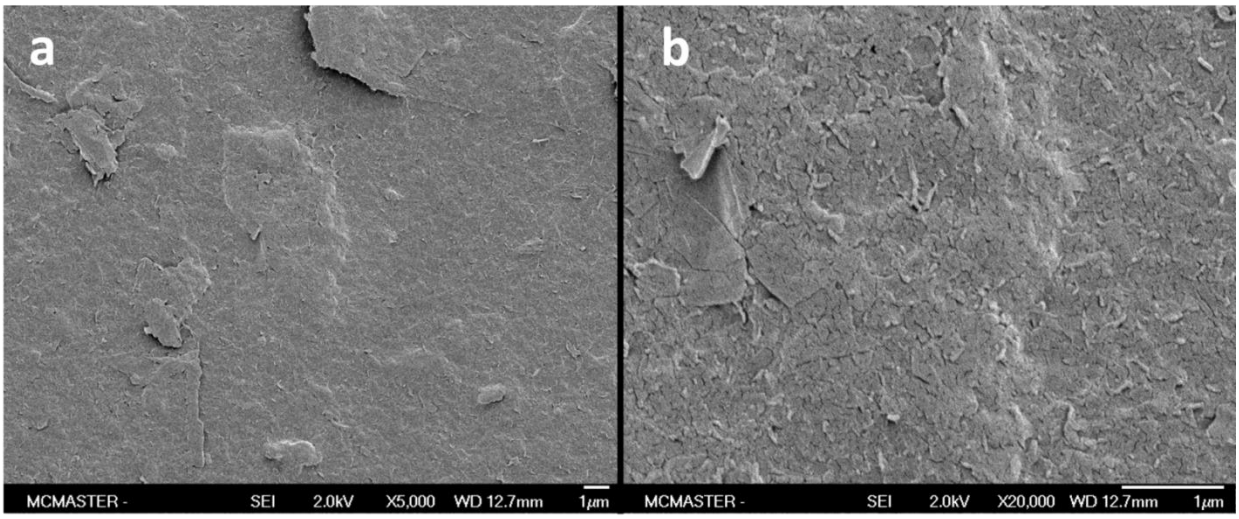

Figure 3-28 a) SEM micrograph using X5000 b) SEM micrograph using X20000.

The dense structure and packed morphology of the surface can be seen in the scanning electron microscope images in Figure 3-28. This is a result of decomposition of EC. As explained earlier, EC would completely decompose for temperatures higher than 450 ^{o}C. The low quality carbon char left behind could both densify the whole structure and fill up the pores between graphene platelets, which reduces the surface area and deteriorates the conductivity of the active material in comparison with pristine, uniform and well connected graphene structure. Other researchers have tried to overcome this challenge by introducing other agents to graphene paper structure in order to increase the layer spacing and make the overall structure less dense and more porous [24, 65, 66].

When the capacitance and SEM results are taken together, we can conclude that the densified morphology and compositional decomposition of the present graphene paper caused by high temperature annealing is not amenable to be used for supercapacitance applications.

Chapter 4: Conclusions and Recommendations

4.1 Conclusions

The current study which focused on the characterization of graphene paper for flexible electronics application has led to the following conclusions:

1- High quality graphene powder can be produced by liquid phase exfoliation of graphite and stable graphene ink can be prepared using appropriate solvents. Furthermore, uniform large scale depositions (~10 cm^2) can be achieved by adjusting the viscosity of the ink (7 ml cyclohexanane and 3 ml terpineol).

2- Based on the statistical modeling of sheet resistance measurements, it was found that the sheet resistance of graphene paper can be reduced from being non-conductive to 150 ohm simply by annealing at 300 ^oC up to 24 hours. This results in the resistivity as low as 42×10^{-6} $ohm.m$. This was attributed to the presence of EC in the chemical composition of the powder as a stabilizing polymer. The annealing time, annealing temperature, and concentration of the as prepared ink are the main variables in the preparation process. Statistical analysis found that third order interaction between these parameters to be the most significant factor contributing to the value of the sheet resistance.

3- Results of two mechanical tests, cyclic bending and adhesion, suggest that the structure of graphene paper gets weaker and more brittle as the annealing time increases. However, samples annealed for 8 hours or less at 300 ^oC showed minimal electrical resistance change after applying either 400 bending cycles or 12 N shear force onto the surface of the samples.

4- Graphene paper developed would appear to be an excellent candidate material for flexible electronics applications where electrical conductivity is needed. This includes interconnects. However, simple capacitance tests of the produced graphene paper indicated that the material does not behave as an ideal double layer supercapacitor. It is suggested that the char left behind by EC decomposition fills up the pores between graphene nano platelets, hence decreasing the surface area and capacitance.

4.2 Recommendations

To further advance this topic of study, it is recommended that more work is undertaken to:

1- Implement a practical higher volume fabrication method to uniformly coat the selected substrate with higher concentrations of graphene ink and greater coating thickness. Although the current method used can produce relatively large size graphene paper areas, a more automated and controlled technique would be required to exploit this material at larger industrial scales.

2- Develop a direct, safe, and high yield procedure to synthesize high quality graphene powder in relatively large amounts. Although some techniques have been advanced especially in liquid phase exfoliation, the lack of high quality material at large scales is a barrier for industrial manufacturing.

3- Thoroughly investigate the interaction between graphene products and their substrates. The resistivity of graphene products is expected to have a practical limit that would restrict their adoption in flexible electronics. Therefore, substrate modification technologies that can increase charge carriers could become critical such as introducing specific doping materials to the substrates.

Bibliography

[1] C. Lee, X. Wei, J. W. Kysar and J. Hone, "Measurement of the Elastic Properties and Intrinsic Strength of Monolayer Graphene," *Science,* vol. 321, pp. 385-388, 07/18, 2008.

[2] K. S. Novoselov, V. I. Fal[prime]ko, L. Colombo, P. R. Gellert, M. G. Schwab and K. Kim, "A roadmap for graphene," *Nature,* vol. 490, pp. 192-200, 10/11, 2012.

[3] S. Lee, J. Kim and J. Ahn, "Graphene as a flexible electronic material: mechanical limitations by defect formation and efforts to overcome," *Materials Today,* vol. 18, pp. 336-344, 0, 2015.

[4] S. De and J. N. Coleman, "Are There Fundamental Limitations on the Sheet Resistance and Transmittance of Thin Graphene Films?" *ACS Nano,* vol. 4, pp. 2713-2720, 05/25, 2010.

[5] M. J. Allen, V. C. Tung and R. B. Kaner, "Honeycomb Carbon: A Review of Graphene," *Chem. Rev.,* vol. 110, pp. 132-145, 01/13, 2010.

[6] W. Choi, I. Lahiri, R. Seelaboyina and Y. S. Kang, "Synthesis of Graphene and Its Applications: A Review," *Critical Reviews in Solid State and Materials Sciences,* vol. 35, pp. 52-71, 02/11, 2010.

[7] M. Yi and Z. Shen, "A review on mechanical exfoliation for the scalable production of graphene," *J. Mater. Chem. A,* vol. 3, pp. 11700-11715, 2015.

[8] K. S. Novoselov, A. K. Geim, S. V. Morozov, D. Jiang, Y. Zhang, S. V. Dubonos, I. V. Grigorieva and A. A. Firsov, "Electric Field Effect in Atomically Thin Carbon Films," *Science,* vol. 306, pp. 666-669, 10/21, 2004.

[9] X. L. and, "Tailoring graphite with the goal of achieving single sheets," *Nanotechnology,* vol. 10, pp. 269, 1999.

[10] W. S. Hummers and R. E. Offeman, "Preparation of Graphitic Oxide," *J. Am. Chem. Soc.,* vol. 80, pp. 1339-1339, 03/01, 1958.

[11] A. Buchsteiner, A. Lerf and J. Pieper, "Water Dynamics in Graphite Oxide Investigated with Neutron Scattering," *J Phys Chem B,* vol. 110, pp. 22328-22338, 11/01, 2006.

[12] J. I. Paredes, S. Villar-Rodil, A. MartÃnez-Alonso and J. M. D. TascÃ³n, "Graphene Oxide Dispersions in Organic Solvents," *Langmuir,* vol. 24, pp. 10560-10564, 10/07, 2008.

[13] M. J. McAllister, J. Li, D. H. Adamson, H. C. Schniepp, A. A. Abdala, J. Liu, M. Herrera-Alonso, D. L. Milius, R. Car, R. K. Prud'homme and I. A. Aksay, "Single Sheet Functionalized Graphene by Oxidation and Thermal Expansion of Graphite," *Chem. Mater.,* vol. 19, pp. 4396-4404, 09/01, 2007.

[14] Y. ZHANG, L. ZHANG and C. ZHOU, "Review of Chemical Vapor Deposition of Graphene and Related Applications," vol. 46, 2013.

[15] S. Bae, H. Kim, Y. Lee, X. Xu, J. Park, Y. Zheng, J. Balakrishnan, T. Lei, H. Ri Kim, Y. I. Song, Y. Kim, K. S. Kim, B. Ozyilmaz, J. Ahn, B. H. Hong and S. Iijima, "Roll-to-roll production of 30-inch graphene films for transparent electrodes," *Nat Nano,* vol. 5, pp. 574-578, print, 2010.

[16] Y. Hernandez, V. Nicolosi, M. Lotya, F. M. Blighe, Z. Sun, S. De, McGovernI. T., B. Holland, M. Byrne, Y. K. Gun'Ko, J. J. Boland, P. Niraj, G. Duesberg, S. Krishnamurthy, R. Goodhue, J. Hutchison, V. Scardaci, A. C. Ferrari and J. N. Coleman, "High-yield production of graphene by liquid-phase exfoliation of graphite," *Nat Nano,* vol. 3, pp. 563-568, print, 2008.

[17] J. N COLEMAN, "Liquid Exfoliation of Defect-Free Graphene," vol. 46, 2013.

[18] R. Lakes, "Materials with structural hierarchy," *Nature,* vol. 361, pp. 511-515, 02/11, 1993.

[19] F. Barthelat, H. Tang, P. D. Zavattieri, C. -. Li and H. D. Espinosa, "On the mechanics of mother-of-pearl: A key feature in the material hierarchical structure," *J. Mech. Phys. Solids,* vol. 55, pp. 306-337, 2, 2007.

[20] H. Chen, M. B. Müller, K. J. Gilmore, G. G. Wallace and D. Li, "Mechanically Strong, Electrically Conductive, and Biocompatible Graphene Paper," *Adv Mater,* vol. 20, pp. 3557-3561, 2008.

[21] Y. Liu, B. Xie, Z. Zhang, Q. Zheng and Z. Xu, "Mechanical properties of graphene papers," *J. Mech. Phys. Solids,* vol. 60, pp. 591-605, 4, 2012.

[22] C. Vallés, J. David Núñez, A. M. Benito and W. K. Maser, "Flexible conductive graphene paper obtained by direct and gentle annealing of graphene oxide paper," *Carbon,* vol. 50, pp. 835-844, 3, 2012.

[23] G. Xin, H. Sun, T. Hu, H. R. Fard, X. Sun, N. Koratkar, T. Borca-Tasciuc and J. Lian, "Large-Area Freestanding Graphene Paper for Superior Thermal Management," *Adv Mater,* vol. 26, pp. 4521-4526, 2014.

[24] Z. Weng, Y. Su, D. Wang, F. Li, J. Du and H. Cheng, "Graphene–Cellulose Paper Flexible Supercapacitors," *Advanced Energy Materials,* vol. 1, pp. 917-922, 2011.

[25] V. Dua, S. Surwade, S. Ammu, S. Agnihotra, S. Jain, K. Roberts, S. Park, R. Ruoff and S. Manohar, "All-Organic Vapor Sensor Using Inkjet-Printed Reduced Graphene Oxide," *Angewandte Chemie International Edition,* vol. 49, pp. 2154-2157, 2010.

[26] M. Huang, H. Yan, C. Chen, D. Song, T. F. Heinz and J. Hone, "Phonon softening and crystallographic orientation of strained graphene studied by Raman spectroscopy," *Proceedings of the National Academy of Sciences,* vol. 106, pp. 7304-7308, May 05, 2009.

[27] C. Xu, T. Xue, J. Guo, Q. Qin, S. Wu, H. Song and H. Xie. An experimental investigation on the mechanical properties of the interface between large-sized graphene and a flexible substrate. *J. Appl. Phys. 117(16),* pp. 164301. 2015. . DOI: http://dx.doi.org/10.1063/1.4918899.

[28] L. Gong, I. A. Kinloch, R. J. Young, I. Riaz, R. Jalil and K. S. Novoselov, "Interfacial Stress Transfer in a Graphene Monolayer Nanocomposite," *Adv Mater,* vol. 22, pp. 2694-2697, 2010.

[29] T. Jiang, R. Huang and Y. Zhu, "Interfacial Sliding and Buckling of Monolayer Graphene on a Stretchable Substrate," *Advanced Functional Materials,* vol. 24, pp. 396-402, 2014.

[30] I. A. Ovidko, "Mechanical Properties of Graphene," vol. 34, 2013.

[31] P. Zhang, L. Ma, F. Fan, Z. Zeng, C. Peng, P. E. Loya, Z. Liu, Y. Gong, J. Zhang, X. Zhang, P. M. Ajayan, T. Zhu and J. Lou, "Fracture toughness of graphene," *Nature Communications,* vol. 5, pp. 3782, 04/29, 2014.

[32] Eva Y Andrei and Guohong Li and,Xu Du, "Electronic properties of graphene: a perspective from scanning tunneling microscopy and magnetotransport," *Reports on Progress in Physics,* vol. 75, pp. 056501, 2012.

[33] K. I. Bolotin, K. J. Sikes, Z. Jiang, M. Klima, G. Fudenberg, J. Hone, P. Kim and H. L. Stormer, "Ultrahigh electron mobility in suspended graphene," *Solid State Commun.,* vol. 146, pp. 351-355, 6, 2008.

[34] K. L. Mittal, "Adhesion Measurement of Thin Films," *ElectroComponent Science and Technology,* vol. 3, pp. 21-42, 1976.

[35] E. Jabari, "Additive Manufacturing of Graphene-based Patterns," 2016.

[36] A. H. Castro Neto, F. Guinea, N. M. R. Peres, K. S. Novoselov and A. K. Geim, "The electronic properties of graphene," *Rev. Mod. Phys.,* vol. 81, pp. 109-162, 01/14, 2009.

[37] F. Liu, S. Song, D. Xue and H. Zhang, "Folded Structured Graphene Paper for High Performance Electrode Materials," *Adv Mater,* vol. 24, pp. 1089-1094, 2012.

[38] E. B. Secor, P. L. Prabhumirashi, K. Puntambekar, M. L. Geier and M. C. Hersam, "Inkjet Printing of High Conductivity, Flexible Graphene Patterns," *J. Phys. Chem. Lett.,* vol. 4, pp. 1347-1351, 04/18, 2013.

[39] W. J. Hyun, O. O. Park and B. D. Chin, "Foldable Graphene Electronic Circuits Based on Paper Substrates," *Adv Mater,* vol. 25, pp. 4729-4734, 2013.

[40] J. Wang, M. Liang, Y. Fang, T. Qiu, J. Zhang and L. Zhi, "Rod-Coating: Towards Large-Area Fabrication of Uniform Reduced Graphene Oxide Films for Flexible Touch Screens," *Adv Mater,* vol. 24, pp. 2874-2878, 2012.

[41] T. Reddy, "Electrochemical capacitors," in *Linden's Handbook of Batteries*, 4th ed.Anonymous McGraw Hill Professional, 2010, .

[42] E. Jabari and E. Toyserkani, "Micro-scale aerosol-jet printing of graphene interconnects," *Carbon,* vol. 91, pp. 321-329, 9, 2015.

[43] Y. Hernandez, M. Lotya, D. Rickard, S. D. Bergin and J. N. Coleman, "Measurement of Multicomponent Solubility Parameters for Graphene Facilitates Solvent Discovery," *Langmuir,* vol. 26, pp. 3208-3213, 03/02, 2010.

[44] M. Yi, Z. Shen, X. Zhang and S. Ma, "Vessel diameter and liquid height dependent sonication-assisted production of few-layer graphene," *J. Mater. Sci.,* vol. 47, pp. 8234-8244, 2012.

[45] H. L. Cai and Y. Xun, "Silver nanowire-based transparent, flexible, and conductive thin film," 2011.

[46] A. A. Tracton, *Coatings Technology: Fundamentals, Testing, and Processing Techniques.* CRC Press, 2006.

[47] DuPont, "Physical and Thermal Properties of Kapton® polyimide films," .

[48] W. S. Wong and A. Salleo, *Flexible Electronics: Materials and Applications.* Springer US, 2009.

[49] C. P. Firme III and P. R. Bandaru, "Toxicity issues in the application of carbon nanotubes to biological systems," *Nanomedicine: Nanotechnology, Biology and Medicine,* vol. 6, pp. 245-256, 4, 2010.

[50] S. Bellucci, *Nanoparticles and Nanodevices in Biological Applications: The INFN Lectures* -. Springer Berlin Heidelberg, 2008.

[51] X. Zhao and R. Liu, "Recent progress and perspectives on the toxicity of carbon nanotubes at organism, organ, cell, and biomacromolecule levels," *Environ. Int.,* vol. 40, pp. 244-255, 4, 2012.

[52] K. Liao, Y. Lin, C. W. Macosko and C. L. Haynes, "Cytotoxicity of Graphene Oxide and Graphene in Human Erythrocytes and Skin Fibroblasts," *ACS Appl. Mater. Interfaces,* vol. 3, pp. 2607-2615, 07/27, 2011.

[53] (). *Nanomaterials Safety Program*.

[54] D. K. Schroder, *Semiconductor Material and Device Characterization.* Wiley, 2006.

[55] A. Yu, I. Roes, A. Davies and Z. Chen. Ultrathin, transparent, and flexible graphene films for supercapacitor application. *Appl. Phys. Lett. 96(25),* pp. 253105. 2010. . DOI: http://dx.doi.org/10.1063/1.3455879.

[56] T. Chen, H. Peng, M. Durstock and L. Dai, "High-performance transparent and stretchable all-solid supercapacitors based on highly aligned carbon nanotube sheets," *Scientific Reports,* vol. 4, pp. 3612, 01/09, 2014.

[57] J. Li, F. Ye, S. Vaziri, M. Muhammed, M. C. Lemme and M. Östling, "Efficient Inkjet Printing of Graphene," *Adv Mater,* vol. 25, pp. 3985-3992, 2013.

[58] D. Kong, L. T. Le, Y. Li, J. L. Zunino and W. Lee, "Temperature-Dependent Electrical Properties of Graphene Inkjet-Printed on Flexible Materials," *Langmuir,* vol. 28, pp. 13467-13472, 09/18, 2012.

[59] E. T. Elahe Jabari and, "Laser heat treatment of aerosol-jet additive manufactured graphene patterns," *J. Phys. D,* vol. 48, pp. 375503, 2015.

[60] A. R. Ranjbartoreh, B. Wang, X. Shen and G. Wang. Advanced mechanical properties of graphene paper. *J. Appl. Phys. 109(1),* pp. 014306. 2011. . DOI: http://dx.doi.org/10.1063/1.3528213.

[61] M. Davidovich-Pinhas, S. Barbut and A. G. Marangoni, "Physical structure and thermal behavior of ethylcellulose," *Cellulose,* vol. 21, pp. 3243-3255, 2014.

[62] X. Li, M. Huang and H. Bai, "Thermal decomposition of cellulose ethers," *J Appl Polym Sci,* vol. 73, pp. 2927-2936, 1999.

[63] A. C. Ferrari, J. C. Meyer, V. Scardaci, C. Casiraghi, M. Lazzeri, F. Mauri, S. Piscanec, D. Jiang, K. S. Novoselov, S. Roth and A. K. Geim, "Raman Spectrum of Graphene and Graphene Layers," *Phys. Rev. Lett.,* vol. 97, pp. 187401, 10/30, 2006.

[64] M. Wall and Thermo Fisher Scientific, "The Raman Spectroscopy of Graphene and the Determination of Layer Thickness," 2011.

[65] H. Cong, X. Ren, P. Wang and S. Yu, "Flexible graphene-polyaniline composite paper for high-performance supercapacitor," *Energy Environ. Sci.,* vol. 6, pp. 1185-1191, 2013.

[66] G. Wang, X. Sun, F. Lu, H. Sun, M. Yu, W. Jiang, C. Liu and J. Lian, "Flexible Pillared Graphene-Paper Electrodes for High-Performance Electrochemical Supercapacitors," *Small,* vol. 8, pp. 452-459, 2012.

Appendix: Copyright Permission

Title: Micro-scale aerosol-jet printing of graphene interconnects
Author: Elahe Jabari,Ehsan Toyserkani
Publication: Carbon
Publisher: Elsevier
Date: September 2015

Order Completed

Thank you for your order.

This Agreement between Kamyar Karimi ("You") and Elsevier ("Elsevier") consists of your license details and the terms and conditions provided by Elsevier and Copyright Clearance Center.

Your confirmation email will contain your order number for future reference.

Get the printable license.

License Number	3943221014414
License date	Sep 06, 2016
Licensed Content Publisher	Elsevier
Licensed Content Publication	Carbon
Licensed Content Title	Micro-scale aerosol-jet printing of graphene interconnects
Licensed Content Author	Elahe Jabari,Ehsan Toyserkani
Licensed Content Date	September 2015
Licensed Content Volume	91
Licensed Content Issue	n/a
Licensed Content Pages	9
Type of Use	reuse in a thesis/dissertation
Portion	figures/tables/illustrations
Number of figures/tables/illustrations	4
Format	both print and electronic
Are you the author of this Elsevier article?	No
Will you be translating?	No
Order reference number	
Original figure numbers	
Title of your thesis/dissertation	The Characterization of Graphene Paper for Flexible Electronics Application
Expected completion date	Sep 2016
Estimated size (number of pages)	90
Elsevier VAT number	GB 494 6272 12
Requestor Location	Kamyar Karimi 107-510 Glenelm Cres Waterloo, ON N2L5C8 Canada Attn: Kamyar Karimi